VANADIUM SELENIUM OXIDE BASED THIN FILM BY SILAR METHOD FOR SUPERCAPACITOR APPLICATION

Dissertation submitted to
Visvesvaraya National Institute of Technology, Nagpur
in partial fulfillment of the requirements for the award of
the degree

Master of Science
in
Physics

by
RAMCHANDRA DASHRATH SHINDE
(MS23PHY002)

under the guidance of

Dr. Babasaheb R. Sankapal
Professor

Department of Physics
Visvesvaraya National Institute of Technology Nagpur 440 010 (India)

May 2025

VANADIUM SELENIUM OXIDE BASED THIN FILM BY SILAR METHOD FOR SUPERCAPACITOR APPLICATION

Dissertation submitted to
Visvesvaraya National Institute of Technology, Nagpur
in partial fulfillment of the requirements for the award of
the degree

Master of Science
in
Physics

by

RAMCHANDRA DASHRATH SHINDE
(MS23PHY002)

under the guidance of

Dr. Babasaheb R. Sankapal
Professor

Department of Physics
Visvesvaraya National Institute of Technology Nagpur 440 010 (India)
(

May 2025

© Visvesvaraya National Institute of Technology (VNIT) 2025

Department of Physics
Visvesvaraya National Institute of Technology,
Nagpur

Declaration

I, **Ramchandra Dashrath Shinde**, hereby declare that this dissertation titled **"Vanadium selenium oxide based thin film by SILAR method for supercapacitor application"** is carried out by me in the Department of Physics of Visvesvaraya National Institute of Technology, Nagpur. The work is original and has not been submitted earlier whole or in part for the award of any degree/diploma at this or any other Institution / University.

Ramchandra Dashrath Shinde
Date:

Certificate

This to certify that the dissertation titled **"Vanadium selenium oxide based thin film by SILAR method for supercapacitor application**" is submitted by **Ramchandra Dashrath Shinde** in partial fulfillment of the requirements for the award of the degree of **Master of Science in Physics**, VNIT Nagpur. The work is comprehensive, complete and fit for final evaluation.

Dr. Babasaheb R. Sankapal
Professor

Head, Department of Physics
VNIT, Nagpur

Date

Department of Physics

Visvesvaraya National Institute of Technology, Nagpur

Non-Plagiarism Certificate

Certified that M.Sc. Dissertation titled **"Vanadium selenium oxide based thin film by SILAR method for supercapacitor application"** submitted by **Ramchandra Dashrath Shinde**, Enrollment no. **MS23PHY002,** ID No.**30081** has been checked for plagiarism using TURNITIN software and overlap is found within prescribed limits (< 30%). A summary of the report given below:

ORIGINALITY REPORT

23%	18%	18%	%
SIMILARITY INDEX	INTERNET SOURCES	PUBLICATIONS	STUDENT PAPERS

Ramchandra Dashrath Shinde
(MS23PHY002)
ID No: 30081

Dr. Babasaheb R. Sankapal
Professor

Acknowledgment

I want to extend my heartfelt thanks to my guide, **Dr. B. R. Sankapal**, Professor and Head of the Department of Physics at Visvesvaraya National Institute of Technology, Nagpur, for giving me the valuable opportunity to undertake this research project and for introducing me to the laboratory environment. This experience greatly enhanced my understanding of the research in Materials Science and will undoubtedly benefit me in the future. It has been a true honor and privilege to work under his guidance. The author acknowledges the DST-FIST project (SR/FST/PSI/2017/5(C)) projects. I would also like to thank all teaching and non-teaching staff of the Physics department, VNIT Nagpur. I would like to thank Mr. T Kedara Shivasharma, Mr. Rajulal Sahu, Mr. Vinay Soni, Mr. Mayur Thosare, Ms. Sapna, and Mr. Raunak Tolani for their guidance, motivation, and continuous support throughout the project work.

My heartfelt appreciation goes to VSM, who provided financial support throughout my master's degree, my father Dashrath Shinde, my mother Sindhu Shinde, my brother Tukaram Shinde, and my other family members, Akshay, Deepak, and Deepali, for their love, affection, and constant support. I am grateful to my colleagues, Mr. Kaushal Joshi, Mr. Himanshu, Mr. Aman, Mr. Ankan, and Mr. Vaibhav for their support and help. I am extremely thankful to my friends Ashish, Amar, Vaibhav, Amritanshu, Banty, and Siddharth for their continuous motivation, inspiration, support, and help.

I'm thankful to the source of creation, if there is any, which gave and continues to give me a chance to take every single breath. My gratitude comes not from belief, but from wonder at how unlikely and vast existence is. In this short moment of being alive, I see how much is beyond our control, yet it still gives us the chance to experience life.

Abstract

Energy storage devices require the creation of nanostructured materials using straightforward, affordable, and industrially scalable deposition methods. Recently, metal chalcogenides have been shown to be useful materials for supercapacitors. They outperform in terms of power and energy density. Vanadium selenium oxide thin film is deposited using the successive ionic layer adsorption and reaction (SILAR) method as an active electrode material in supercapacitor applications. The structure of the produced samples is analyzed using X-ray diffraction characterisation. Surface wettability is investigated by taking the contact angle measurement. The bond vibrations were analyzed by Fourier transform infrared spectroscopy.

The electrochemical studies showed the working potential of the electrode is 2.2 V (-0.7V to 1.5 V) in 0.5 M $NaClO_4$ solution with acetonitrile as a solvent. According to the GCD studies, the maximum areal capacitance of 45.59 mF/cm^2 at 1 mA/cm^2 with a working potential range of -0.7 V to 1.5 V, while the electrochemical CV studies demonstrate a maximum areal capacitance of 450.72 mF/cm^2 at a scan rate of 2 mV/s. 83.86% retention in the areal capacitance after 1000 charge-discharge cycles was recorded. Electrochemical impedance spectroscopy measurement was carried out to understand the overall behavior of the electrochemical system

LIST OF FIGURES

Figure No.	Figure Title	Page No.
Figure 1.1	Energy storage devices	2
Figure 1.2	Ragone plot for different energy storage devices	4
Figure 1.3	Types of supercapacitors	5
Figure 1.4	Diagram of electric double layer capacitor	6
Figure 1.5	Diagram of Pseudocapacitor (a) Faradaic process (b) Intercalation	7
Figure 1.6	Work plan	11
Figure 2.1	Thin film deposition methods	12
Figure 2.2	SILAR deposition	13
Figure 2.3	Experimental SILAR set-up	14
Figure 2.4	Contact angle measurement	17
Figure 2.5	Reflection of X-rays from planes	18
Figure 2.6	X-ray diffractometer	19
Figure 2.7	Schematic of Fourier transform infrared spectroscopy	20
Figure 2.8	Schematic of SEM	21
Figure 2.9	Schematic of potentiostat with 3-electrode configuration	22
Figure 2.10	CV curve of a reversible single electrode reaction.	23
Figure 2.11	Electrochemical impedance spectroscopy	26
Figure 3.1	Contact angle measurements of (a) SS with DDW, (b) SS/ $V_2(Se_2O_9)$ with DDW	30

Figure 3.2	XRD pattern of $V_2(Se_2O_9)$ sample	31
Figure 3.3	Fourier transform infrared spectroscopy of $V_2(Se_2O_9)$ sample	32
Figure 3.4	SEM images of $V_2(Se_2O_9)$ for (a) 50, (b)75 and (c)100 SILAR cycles and fig. (d) and (e) shows images at 100 nm for 75 and 100 SILAR cycles respectively.	33
Figure 3.5	a) CV curves of in $LiClO_4$ and $NaClO_4$ electrolytes, (b) Areal capacitance for $LiClO_4$ and $NaClO_4$ electrolytes	34
Figure 3.6	(a) CV curves with different concentration of $NaClO_4$, (b) Specific capacitance vs concentration.	35
Figure 3.7	(a) CV curves with different SILAR cycles, (b) Areal capacitance at different SILAR cycles	35
Figure 3.8	(a) CV plots at different scan rates, (b) Areal capacitance at different scan rate	36
Figure 3.9	(a) GCD plots at different current densities, (b) Areal capacitance vs current densities	38
Figure 3.10	(a) CV plots at different number of cycles, (b) Capacitance retention vs number of cycles.	38
Figure 3.11	Nyquist plot and inset shows equivalent circuit	39

LIST OF TABLES

Table No.	Table Name	Page No.
Table 1.1	Comparison between capacitors, supercapacitors and Batteries	5
Table 1.2	Summarized supercapacitor performance of Vanadium selenides and vanadium oxides	8
Table 1.3	Properties of $V_2(Se_2O_9)$	10
Table 3.1	Preparative parameters for the deposition of $V_2(Se_2O_9)$ thin Film	29
Table 3.2	Electrochemical impedance spectroscopy measurements	39
Table 4.1	Parameters of preparation for the deposition of $V_2(Se_2O_9)$ thin Film	41
Table 4.2	Contact angle experiment	41
Table 4.3	XRD peaks and respective planes of $V_2(Se_2O_9)$	42
Table 4.4	Fourier transform infrared spectroscopy analysis	42
Table 4.5	Areal Capacitance of $V_2(Se_2O_9)$ in different electrolytes at 100mV/s	43
Table 4.6	Areal Capacitance of $V_2(Se_2O_9)$ in $NaClO_4$ at different concentrations at 100 mV/s.	44
Table 4.7	Areal capacitance of $V_2(Se_2O_9)$ deposited with different SILAR cycles at 100 mV/s	44

Table 4.8	Areal capacitance of $V_2(Se_2O_9)$ with different scan rate	45
Table 4.8	Areal capacitance of $V_2(Se_2O_9)$ at different current densities	45

Notations

Notations	Description
$V_2(Se_2O_9)$	Vanadium selenium oxide
C	Capacitance
Q	Charge
V	Voltage
ε	Dielectric constant
A	Surface area
d	Thickness of dielectric
ESR	Equivalent series resistance
P_{max}	Maximum power
E	Energy density
P	Power density
t	Time
EDLC	Electric double layer capacitor
SS	Stainless steel
SILAR	Successive ionic layer adsorption and reaction
SS/ $V_2(Se_2O_9)$	$V_2(Se_2O_9)$ deposited stainless steel substrate
CBD	Chemical bath deposition
$VOSO_4$	Vanadyl sulphate
Na_2SO_3	Sodium sulfite

Na_2SeSO_3	Sodium selenosulfate
DDW	Double distilled water
XRD	X-ray diffraction
JCPDS	Joint committee on powder diffraction standards
CV	Cyclic voltammetry
GCD	Galvanostatic charge-discharge
WE	Working electrode
RE	Reference electrode
CE	Counter electrode
C_S	Specific capacitance
ΔV	Potential window
v	Scan rate
Δt	Discharging time
I	Current density
SE	Specific energy density
SP	Specific power density
ES	Electrospinning
HT	Hydrothermal
NF	Nickel foam
CF	Carbon fiber
SCs	Supercapacitors

PCs	Pseudocapacitors
HCs	Hybrid capacitors
EIS	Electrochemical impedance spectroscopy
IP	Ionic product
Pt	Platinum
PW	Potential window
W	Warburg impedance

INDEX

Sr. No	Title	Page No.
	CHAPTER I **INTRODUCTION TO SUPERCAPACITORS AND LITERATURE SURVEY**	
1.1	General introduction	1
1.2	Energy storage devices 1.2.1 Batteries 1.2.2 Fuel cell 1.2.3 Capacitors 1.2.4 Supercapacitors	1 2 2 2 3
1.3	Types of Supercapacitors 1.3.1 Electric double layer capacitor 1.3.2 Pseudocapacitor 1.3.3 Hybrid capacitor	5 6 7 7
1.4	Supercapacitor material selection	8
1.5	Literature survey	8
1.6	Research gap	9
1.7	Properties of vanadium selenium oxide based material	9
1.8	Electrolyte	10
1.9	Objectives	10

1.10	Work plan	11
	CHAPTER II **THIN FILM DEPOSITION METHODS, CHARACTERIZATION TECHNIQUES AND SUPERCAPACITOR STUDY**	
2.1	Introduction	12
2.2	Successive ionic layer adsorption and reaction (SILAR)	13
	2.2.1 Solubility product and ionic product	14
	2.2.2 Parameters in SILAR	15
	2.2.3 Advantages of SILAR	16
	2.2.4 Disadvantages of SILAR	16
2.3	Thin film characterization techniques	16
	2.3.1 Surface wettability	16
	2.3.2 X-ray diffraction (XRD)	17
	2.3.3 Fourier transform infrared spectroscopy (FTIR)	19
	2.3.4 Scanning electron microscopy (SEM)	20
	2.3.5 Electrochemical characterization	21
	A) Electrochemical experimental setup	22
	B) Cyclic voltammetry (CV)	22
	C) Galvanostatic charge discharge (GCD)	24
	D) Electrochemical impedance spectroscopy (EIS)	25

CHAPTER III

VANADIUM SLENIUM OXIDE BASED THIN FILM BY SILAR METHOD FOR SUPERCAPACITOR APPLICATION

3.1	Introduction	27
3.2	Experimental studies	27
	3.2.1 Materials	27
	3.2.2 Synthesis of V-Se-O based thin film	27
	a) Substate selection and cleaning process	28
	b) Preparation of the precursor.	28
	3.2.3 Thin film of V-Se-O based thin film on stainless steel by SILAR method.	29
3.3	Characterizations	29
3.4	Results and discussions	30
	3.4.1 Surface wettability study	30
	3.4.2 X-ray diffraction analysis (XRD)	31
	3.4.3 Fourier transform infrared spectroscopy (FTIR)	31
	3.4.4 Surface morphological study	32
	3.4.5 Supercapacitor studies of electrode	34
	1. Electrolyte optimization	34
	2. Concentration	34
	3. Effect of number of SILAR cycles variation	35
	4. Effect of scan rate	36
	5. Cyclic stability	36

	6. Effect of current density 7. Electrochemical impedance spectroscopy (EIS)	37 38
CHAPTER IV **SUMMARY AND CONCLUSIONS**		
4.1	Introduction 4.1.1 Deposition of V-Se-O based thin film 4.1.2 Characterization of thin film a) Surface wettability b) X-ray diffraction (XRD) c) Fourier transform infrared spectroscopy (FTIR) d) Scanning electron microscopy (SEM) e) Electrochemical studies	40 41 41 41 42 42 43 44
4.2	Conclusions	46
4.3	Future scope	46
4.3	References	47

CHAPTER I

INTRODUCTION TO SUPERCAPACITORS AND LITERATURE SURVEY

1.1 General introduction

We are all aware of rapid development in industrial infrastructure and technology all over the world, and the simultaneous demand for energy to achieve all human needs is also increasing rapidly. In order to keep growing, we need both the energy generation systems and systems which can store energy and can use that energy efficiently later on. Energy storage technologies are the mediator between energy generation and consumption [1].

Various types of energy storage devices have been developed to meet specific requirements of using energy whenever there is need. Which includes capacitors, batteries, supercapacitors (SCs) or ultracapacitors, and fuel cells. However, there remains a need to identify a storage technology suitable for widespread application. From past few years, electrochemical energy storage systems such as batteries, capacitors, hydrogen storage units, and supercapacitors (SCs) have seen growing demand. Among these, SCs have attracted considerable increased interest over recent years due to their exceptionally high specific power, rapid charging and discharging capabilities, superior cycle life compared to traditional batteries, and greater specific energy compared to conventional capacitors. SCs utilize several mechanisms to store energy, including the electric double layer (EDL) effect, surface redox reactions, and intercalation processes [2], [3].

1.2 Energy storage devices

Mainly, there are two types of charge storage mechanisms, non-faradaic and faradaic mechanisms. In non-faradaic mechanism, there is electrostatic storage of charges at the interfaces of electrode through reversible ion adsorption, while in faradaic process, charge storage is due to the fast and reversible faradaic reactions at the interface of the electrodes

which involves electron transfer reactions (oxidation and reduction) between the electrode and electrolyte [4].

Figure 1.1: Energy storage devices

1.2.1 Batteries

Batteries store energy using chemical reactions that can be reversible. Each battery has one or more cells made up of an anode, a cathode, and an electrolyte. When the battery charges, electrolyte ions are stored at the interface of the electrode and electrolyte, and energy is stored as chemical energy. When the battery is used (discharged), the electrons flow from the anode to the cathode, producing electricity [5].

1.2.2 Fuel cell

Fuel cells produce electricity through a chemical reaction by converting the chemical energy in fuel directly into electrical energy. Fuel cells keep making electricity as long as they are given a constant supply of fuel and oxygen [5].

1.2.3 Capacitors

A capacitor is made up of two conductive plates with an insulating layer, also known

as the dielectric with permittivity (ϵ), placed in between them. When a voltage is applied, opposite charges build up on each plate, which are placed apart, creating an electric field that stores energy. The ability of a capacitor to store charge is called capacitance. It depends on how much charge it can hold at a given voltage. Capacitance increases with a larger plate surface area and decreases as the distance between the two plates or the thickness of the dielectric increases, as there is direct dependance of capacitance on the surface area (A). Mathematically it is given by equation (1.1) [6].

$$C = \frac{Q}{V} = \frac{\epsilon A}{d} \tag{1.1}$$

And energy is given by,

$$E = \frac{CV^2}{2} \tag{1.2}$$

where, C = capacitance, Q = charge stored, V = voltage applied, ϵ = permittivity of dielectric material, A = surface area of the electrode, d = thickness of the dielectric medium [6].

1.2.4 Supercapacitors

SCs, also referred to as ultracapacitors or electrochemical capacitors having high capacitance as compared to conventional capacitor. This enhanced capacitance is primarily because of the utilization of electrode materials with exceptionally high surface areas due to porous nature of materials and the application of ultra-thin dielectric layers. Structurally, supercapacitors (SCs) resemble traditional capacitors, wherein the thin dielectric medium is interposed between two electrodes. However, due to the advanced materials, they are capable of delivering high power output at rapid rates, surpassing typical battery discharge capabilities. Despite this, a major constraint of supercapacitors lies in their relatively limited energy storage capacity as compared to conventional batteries.

As a result, SCs are particularly well-suited for applications demanding quick energy bursts rather than sustained energy supply. They effectively bridge the performance gap in terms of specific power and specific energy between conventional capacitors and batteries. Notable electrochemical advantages of SCs include rapid charge-discharge cycles, superior

cycle life, straightforward and cost-effective fabrication processes, and low maintenance requirements. SCs have demonstrated considerable potential across a broad spectrum of practical applications, particularly in transportation systems and consumer electronics. In the latter, they are commonly employed as supplementary energy sources for devices such as mobile phones, system memory units, microcomputers, motherboards, clocks, and electronic toys. SCs also play an important role in uninterruptible power supply (UPS) systems, where their rapid charge-discharge abilities are highly beneficial [3], [5], [6].

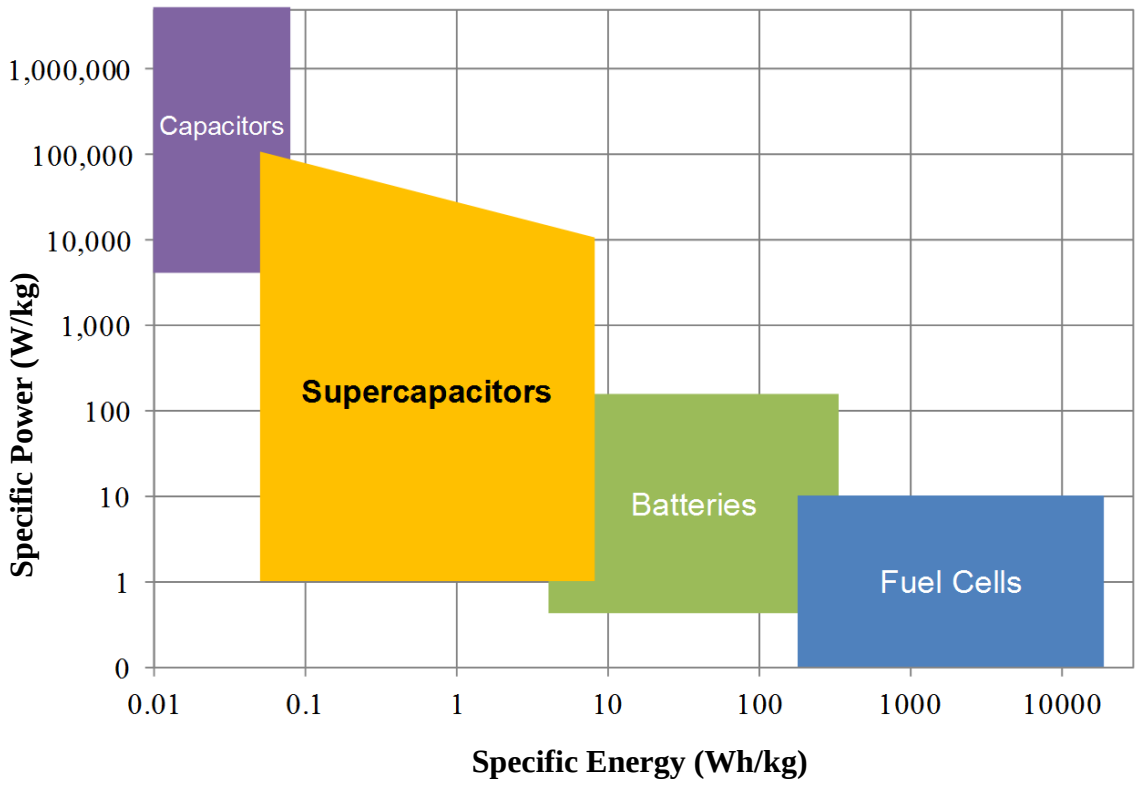

Figure 1.2: Ragone plot for different energy storage devices [7]

Table 1.1: Comparison between the capacitors, supercapacitors and batteries[7], [8], [9].

Characteristics	Capacitor	Supercapacitor	Battery
Specific energy (Wh/kg)	< 0.1	Up to 1.091×10^3	Up to 1.606×10^3
Specific power (W/kg)	$>10^3$	Up to 196×10^3	$< 10^3$
Charge time	10^{-6} to 10^{-3}s	s to min	1-5hr
Discharge time	10^{-6} to 10^{-3}s	s to min	0.003 – 3hr
Life cycle	∞	$>500 \times 10^3$	About $\times 10^3$

1.3 Types of supercapacitors

Figure 1.3: Types of supercapacitors

Mainly there are three types of supercapacitors (SCs), namely; electric double layer capacitors (EDLCs), pseudocapacitors (PCs) and hybrid capacitors (HCs). EDLCs store

charge electrostatically, PCs store charge electrochemically and HCs stores charge both electrostatically as well as electrochemically.

1.3.1 Electric double layer capacitor

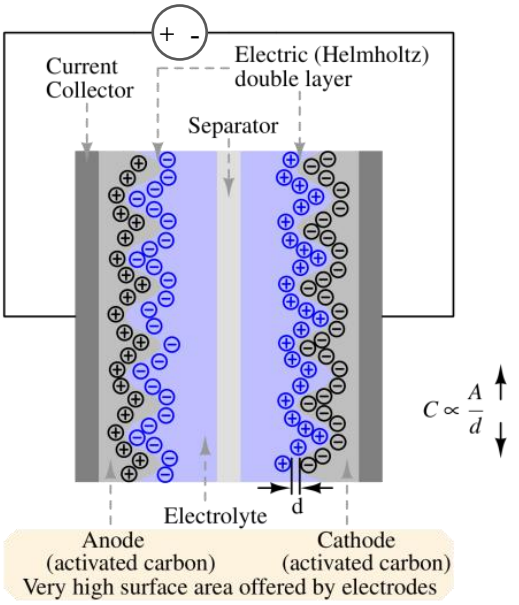

Figure 1.4: Diagram of electric double layer capacitor [10]

Mechanism of charge storage in EDLC is governed by a non-faradaic process, specifically the physical adsorption of electrolyte ions, both cations and anions at the interface of electrode and the electrolyte. This behavior can be effectively described using the Helmholtz double layer model, wherein energy storage arises from electrostatic separation of charges within a naturally formed interfacial double layer. The specific capacitance (Cs) in EDLC is strongly influenced by the electrode's specific surface area and distribution of pore size, with higher surface area materials generally enabling greater capacitance. During the charging phase, electrons are transferred externally from the cathode to the anode, forcing anions in the electrolyte to migrate toward the anode and cations toward the cathode. This ion motion is reversed while discharging. Due to the absence of any chemical transformation or phase transition at the electrode-electrolyte interface, EDLCs exhibit highly reversible operation and prolonged cycle life. Carbon-based porous materials, including carbon aerogels, graphene, activated carbon, carbon nanotubes, and carbon nanofibers are commonly employed as electrode materials owing to their large surface area and superior electrical

conductivity [3], [6], [10].

1.3.2 Pseudocapacitor

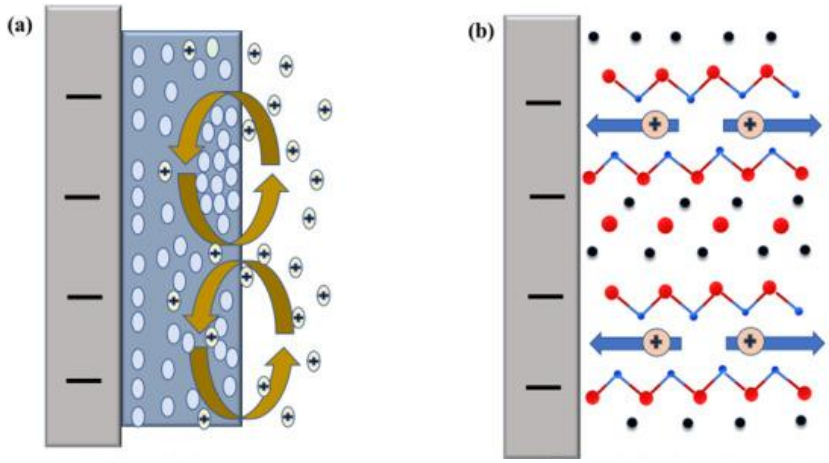

Figure 1.5: Diagram of pseudocapacitor (a) Faradaic process (b) Intercalation [11]

Pseudocapacitor's charge storage mechanism is predominantly governed by faradaic process. Unlike electric double layer capacitors (EDLCs), which rely primarily on electrostatic adsorption, PCs utilize materials that facilitate charge storage through redox reactions, ion intercalation, and adsorption. Although a minor contribution to capacitance may be from the electric double layer, the primary energy storage arises from fast, reversible redox transitions occurring at or near the electrode surface. This faradaic behavior enables PCs to reach higher specific capacitance and energy densities compared to EDLCs. However, the electrochemical reactions involved often lead to structural or compositional changes in the electrode materials, thereby limiting their electrochemical cyclic stability and reducing power density after several charging-discharging cycles. The performance of PCs is influenced by multiple parameters, including electrode surface area, particle size, ionic conductivity of the electrolyte, pore architecture, intrinsic conductivity of the active material, and overall cell design. Materials commonly utilised for pseudocapacitor electrodes include conducting polymers, metal chalcogenides and transition metal oxides, all of which offer high electrochemical activity suitable for redox-based energy storage [10] [2].

1.3.3 Hybrid capacitor

Hybrid supercapacitors (HCs) are a new form of energy storage. It is nothing but a

combination of EDLC and PCs. Unlike other SCs, HCs offer a better balance between energy and power output. They help close the gap in performance that usually exists between batteries and SCs [6].

1.4 Supercapacitor material selection

The electrode material mostly determines the supercapacitors' characteristics. The primary obstacles that SCs must overcome are poor energy density and high cost of manufacturing. One of the best methods to address these problems is to develop new kinds of electrode materials. Because of their enhanced ion adsorption or quicker surface redox reactions, nanomaterials are the perfect supercapacitor materials. Their enhanced active sites for electrochemical reactions enable improved charge transfer mechanism. The most often utilized electrode materials nowadays are conducting polymers, metal oxides, and carbon. The better materials in electrode fabrication are carbon nanomaterials because of their enhanced conductivity, large surface area, outstanding mechanical strength, affordability, and high stability [11]

Metal oxides have minimal equivalent series resistance (ESR) and high conductivity. The high energy density of these materials can be attributed to their high specific capacitance. Nevertheless, metal oxides still fulfil their potential and have a variety of uses. The metal chalcogenides and metal oxides have been the subject of a substantial amount of research in recent years.[12]

1.5 Literature survey

Table 1.2: Summarized supercapacitor performance of vanadium selenides and vanadium oxides.

Material	Method	Substrate	Electrolyte	SC	ED	PD	Stability	Ref.
VSe_2@NC	HT	NF	2 M KOH	313.8 F/g at 1 A/g	85.41 Wh/kg)	701.99 (W/kg)	90% @ 2000	[13]

Mn-VSe_2	HT	NF	0.5 M K_2SO_4	250 F/g at 1 A/g	21.3 Wh/Kg	25.6 kW/kg	95% @ 5000	[14]
VSe_2	HT	NF	1 M KOH + 0.02 M $K_3Fe(CN)_6$	512 F/g at 0.2 mV/s	26 Wh/kg	500 kW/kg	84.7% @ 6500	[15]
VSe_2/SWCNTs/rGO	HT	NF	0.5 M K_2SO_4	450 F/g at 1 A/g	131.4 Wh/kg	27.49 kW/kg	91% @ 5000	[16]
NiVSe–MXene	HT	NF	3 M KOH	305.8 F/g at 1 A/g	***	***	91.7% @ 7000	[17]
V_2O_3	ES	CF	4 M KOH	557 F/g at 0.5 A /g	***	***	***	[18]
V_2O_5	ES	CF	4 M KOH	476 F/g at 0.5 A /g	***	***	***	[18]
VO_2-V_2O_5	ES	CF	4 M KOH	606 F/g at 0.5 A /g	***	***	***	[18]
V_2O_5	ES	Al foil	1 M $LiClO_4$	250 F/g	5 Wh/kg	78 Wh/kg	***	[19]

1.6 Research gap

There is no report on synthesis of V-Se-O based oxide by SILAR method for supercapacitor applications.

1.7 Properties of vanadium selenium oxide based material

The atomic number of vanadium is 23, belongs to Group VB and the fourth period of the periodic table having electronic configuration [Ar] $4s^2$ $3d^3$ [20]. Vanadium can exist in oxidation states of +2, +3, +4 and +5 states are also known [20].

Table 1.3: Properties of $V_2(Se_2O_9)$

Chemical formula	$V_2(Se_2O_9)$
Molar mass	403.8 g/mol

The selenium is a group VIA element in the periodic table with an electronic configuration $[Ar]3d^{10}4s^24p^4$. The atomic number of selenium is 34 and its possible oxidation states are -2, -1, +1, +2, +3, +4, +5, +6.

1.8 Electrolyte

In SCs, the electrolyte is crucial because it allows for charge balancing on each electrode by providing ionic conductivity. The mixture of electrolyte salt and solvent is referred to as the electrolyte. The characteristics of the supercapacitor are influenced by the ion type, size, solute concentration, interaction between ion and solvent, electrolyte-electrode material interaction, and working potential range. In order to create a highly effective device the appropriate electrolyte for a certain electrode can be chosen by researching the interactions between various electrolytes. Reaction of electrode material with an electrolyte after passing current through working electrode is also crucial point while deciding an electrolyte because it should not get dissolve in to the electrolyte after passing current through working electrode. In case of an aqueous electrolyte properties like hydrophilic and hydrophobic need to be consider while selecting an electrolyte. Organic electrolytes give an edge over aqueous electrolytes in terms of potential window and overall electrochemical performance[21].

1.9 Objectives

1. Synthesis of V-Se-O based thin film for supercapacitor application
2. Characterization by X-ray diffraction, surface wettability measurement, and Fourier transform infrared spectroscopy.
3. Electrochemical characterization by galvanostatic charge-discharge, cyclic voltammetry, and electrochemical impedance spectroscopy.
    a) Electrolyte optimization

b) Concentration variation of electrolyte

c) SILAR cycles variation

d) Scan rate variation

e) Current density variation

f) Cyclic stability

g) Electrochemical impedance spectroscopy (EIS)

1.10 Work plan

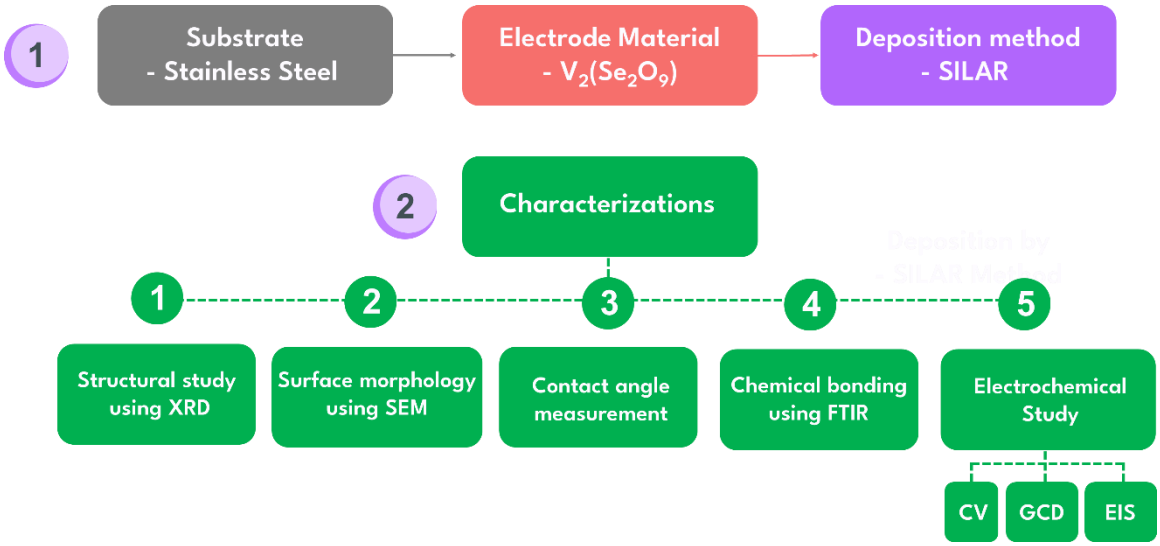

Figure 1.6: Work plan

CHAPTER II

THIN FILM DEPOSITION METHODS, CHARACTERIZATION TECHNIQUES AND SUPERCAPACITOR STUDY

2.1 Introduction

Day by day the technology is rapidly changing, and the materials are also required with new and enhanced properties, with minimum costs and easy to synthesize. Thin films are best to serve this purpose because they use less material, cost-effective synthesis methods and their growth can be easily controlled, allowing us to adjust their properties as per the requirement of application.

Mainly there are two approaches to synthesis materials. Top-down and bottom-up approach. In the top-down approach we crush and grind the particles of materials which are large in size and break them into smaller particles to change their properties as we know properties change as we decrease the size of particles and vice versa. On the other hand,

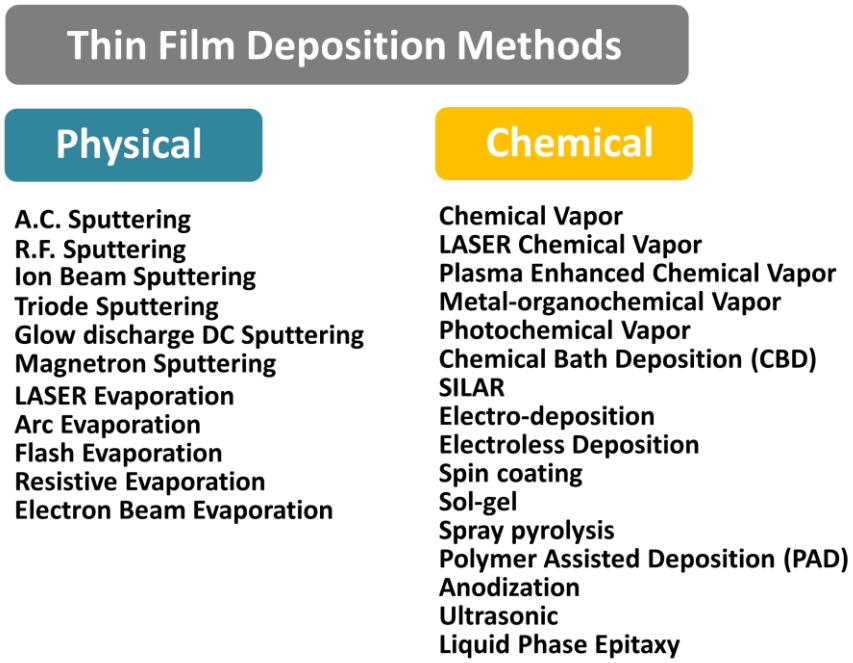

Figure 2.1: Thin film deposition methods

in the bottom-up approach atom by atom we synthesize materials through various methods. Predominantly there are two categories of thin film deposition, physical Methods and chemical methods as shown in Fig. (2.1) [22], [23].

2.2 Successive ionic layer adsorption and reaction (SILAR)

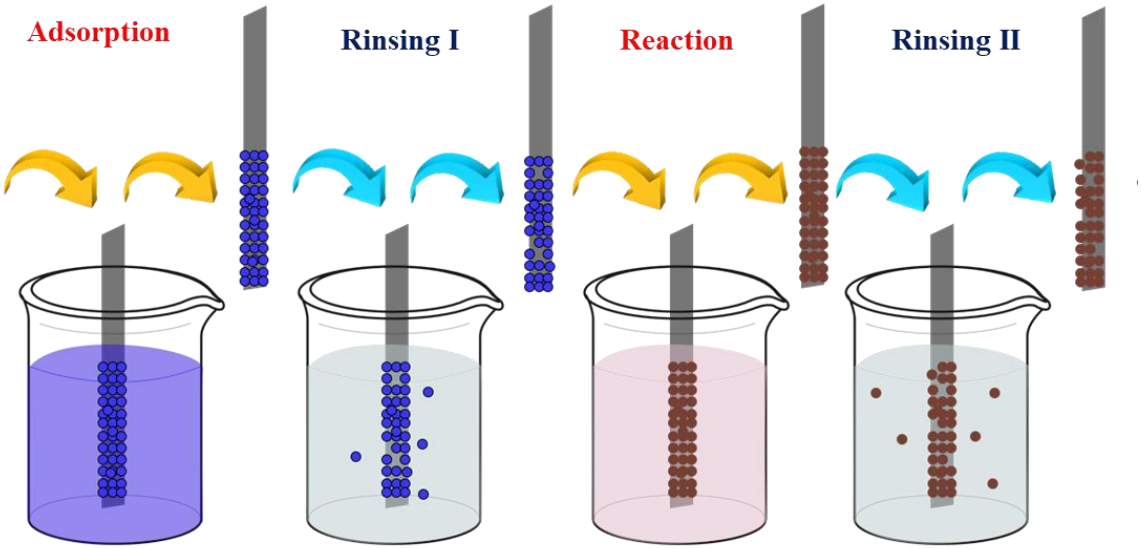

Figure 2.2: SILAR deposition

As the name implies, the SILAR stands for "Successive Ionic Layer Adsorption and Reaction." This method involves alternately dipping a substrate into a cationic solution, where positive ions are adsorbed onto the surface, and then dipping it in an anionic solution, leading to a reaction between the adsorbed cations and incoming anions. This method is among the most straightforward and cost-effective methods for the deposition of thin films and can be used to deposit different kinds of materials. Similar to chemical bath deposition (CBD), the film forms when the ionic product exceeds the solubility product. However, in CBD unwanted bulk precipitation often occurs; SILAR minimizes such issues by controlling reactions on the substrate surface. It works well with a wide range of substrates with the property of insolubility that allows easy interaction with the solution. The main steps in the SILAR process include ion adsorption, first rinsing, ion reaction, and second rinsing as shown in the above Fig. (2.2). The thin film can be deposited by repeating the four steps SILAR cycle for a different number of times and hence, we can get uniform film of desired thickness [24].

1. **Adsorption:** After immersion in first beaker, cations in the cationic solution are

get adsorbed in this part of the process. because of the van der wall forces.

2. **Rinsing I:** In this step, the substrate is dipped in DDW to remove the cations which are loosely adhered to substrate.
3. **Reaction:** In this stage, the pre-adsorbed cations react with anions from the anionic precursor to produce the desired material.
4. **Rinsing II:** In last step, the purpose is to remove the excess, unreacted species, reaction by-product and loosely adhered species.

Figure 2.3: Experimental SILAR set-up

2.2.1 Solubility product and ionic product

Important factors that determine the adhesiveness, stoichiometry, and homogeneity of the deposited films are solubility and ionic products. An equilibrium between the solid salt and the ions in the solution is reached when the sparingly soluble salt AB is mixed with water to create a saturated solution that contains undissolved AB salt along with A^+ and B^- ions.

$$AB \rightleftharpoons A^+ + B^- \tag{2.1}$$

According to the law of mass action,

$$K = [C_{A^+}.C_{B^-}]/\ C_{AB} \tag{2.2}$$

where C_{A^+}, C_{B^-} and C are the concentrations of A^+, B^- and AB in the solution, respectively. The concentration of the pure solid is a constant number i.e., $C_{AB}(S) = K'$.

$$K = [C_{A^+}.C_{B^-}]/K' \quad (2.3)$$

$$K.K' = [C_{A^+}.C_{B^-}] \quad (2.4)$$

As K and K′ are constants, the product (K.K′) is also a constant called solubility product (SP) and denoted by K_S (K_S = K.K′). And the product of cationic and anionic concentrations in solution (C_A^+. C_B^-) is called ionic product (IP). Both ionic and solubility products are equal in saturated solution. However, the solution becomes supersaturated when the ionic product becomes greater than the solubility product (IP > SP) and formation of nuclei starts due to ion to mixing [24].

2.2.2 Parameters in SILAR

1. **Concentration:** The concentration of ions determines film thickness. Higher concentrations speed up the reaction leading to increased film thickness, further increase in the thickness might lead to the peeling off of the deposited film.

2. **Temperature:** Thicker films result from higher temperatures because they accelerate ion dissociation and deposition. When the temperature drops, thickness reduces.

3. **pH:** A higher pH decreases the concentration of metal ions while accelerating processes. Film development may halt if the pH is too high since there won't be enough ionic product.

4. **Complexing agent:** Reduces the rate of reaction, controlled film thickness might be achieved by releasing ions gradually, and forms complexes to control the availability of metal ions.

5. **Number of SILAR cycles:** After a saturation point, too many cycles can result in peeling off the sample from substrate, but more cycles thicken the layer.

2.2.3 Advantages of SILAR

In SILAR without a regulated atmosphere or complex equipment, the ionic layer-by-layer growth increases the film's porosity and compactness, which is why supercapacitors use it. The following are some benefits of the SILAR method:

1. It is simple to regulate the film's shape, stoichiometry, and thickness.
2. It is the simplest and most cost-effective method of applying a thin layer over a broad area.
3. In general, it doesn't need a high temperature like other method do, but we can adjust it based on the kinetics of reaction.
4. Any kind of substrate can be used to deposit film.
5. SILAR does not require a high vacuum atmosphere.
6. The SILAR's ability to reduce chemical loss is one of its key advantages.
7. Adsorption, reaction time or the number of SILAR cycles can all be used to regulate the film's thickness.

2.2.4 Disadvantages of SILAR

1. For the film to form, an anion and cation must react spontaneously.
2. The precursor solution should be such that it permits complete adsorption at the interface of liquid and solid since the SILAR is an adsorption-reaction mechanism.
3. The film's exact structure is hard to control and takes a lot of time [25].

2.3 Thin film characterization techniques

Materials behave differently at the nanoscale than they do in their bulk state. These materials are studied using a variety of characterization techniques to study and to manipulate properties accordingly by varying respective synthetic parameters. Developing and comprehending novel materials has been essential to the advancement of science and technology. In this procedure, characterization is crucial because it offers comprehensive details about the composition, structure, phase, and surface characteristics of thin films.

2.3.1 Surface wettability

The equilibrium between the cohesive forces inside a liquid and the adhesive forces between the liquid and a solid surface is known as surface wettability. It establishes a liquid's

ability to spread out on a surface. The contact angle that forms between the liquid drop and the surface is used to quantify this behavior. When the contact angle is zero degrees, the liquid spreads out completely, indicating that the surface is fully wet. The surface is regarded as super hydrophilic, which means it draws water, if the contact angle is between 0° and 90°. The surface is said to be hydrophobic when the contact angle is greater than 90° and it resists wetting. If angle is greater than or equal to 150^{o} then it superhydrophobic in nature [26].

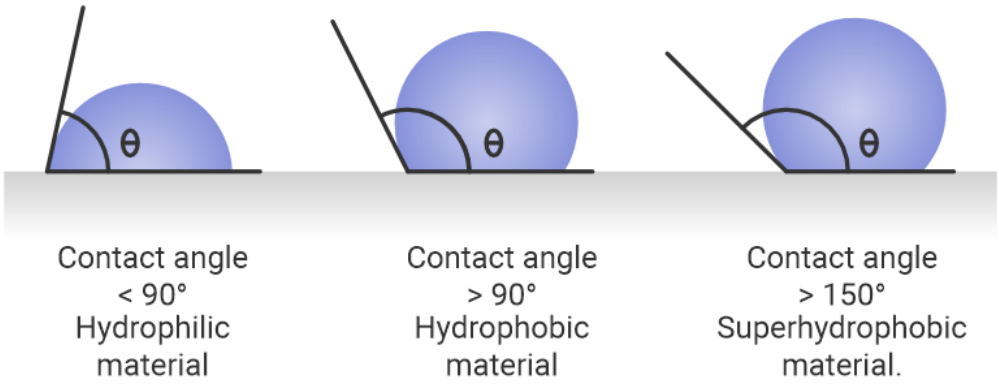

Figure 2.4: Contact angle measurement [27]

2.3.2 X-ray diffraction (XRD)

XRD is the important method for studying materials, specifically material's structure XRD, which is particularly useful for determining their structure. It is like the finger print of materials. It helps in the determination of lattice parameters, internal strain, grain size, interplanar distance between atomic layers, and crystal structure. The measured interplanar distance is compared to standard values published by the Joint Committee on Powder Diffraction Standards (JCPDS) to find the phase present in a synthesized materials or the material under investigation. Atoms are grouped in a repeating pattern within a crystalline solid. A unit cell is the smallest repeating unit. X-rays can reflect off these planes and reveal details about the crystal structure since their wavelengths are comparable to the distances between atomic layers. At some angles known as Bragg angles, constructive interference occurs, in which the X-rays reinforce one another. Destructive interference cancels out the signal at other angles. It is given by Bragg's law, [27]

$$2d\sin\theta = n\lambda \qquad (2.3)$$

Where, λ: wavelength of X-ray, n: order of diffraction, d: distance between atomic planes, θ: diffraction angle. The "Debye-Scherrer formula" is another method that uses the Bragg angle to estimate the size of small crystals in the material is given by, [28]

$$D = \frac{K\lambda}{\beta \cos \theta} \qquad (2.3)$$

Where,

D： Crystallite size

K： Shape factor (0.89 to 1.39; 0.9 is frequently employed)

λ： X − rays wavelength

β： The peak width at half maximum (FWHM)

θ： Bragg angle.

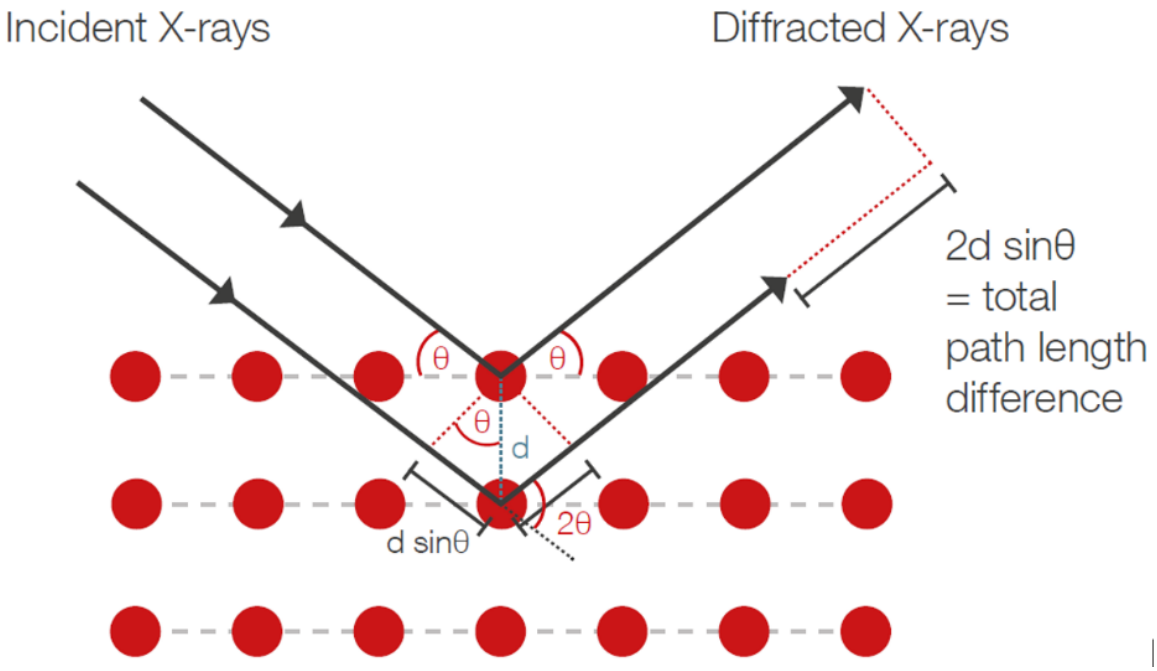

Figure 2.5: Reflection of X-rays from planes [29]

Figure 2.6: X-ray diffractometer [30]

2.3.3 Fourier transform infrared spectroscopy (FTIR)

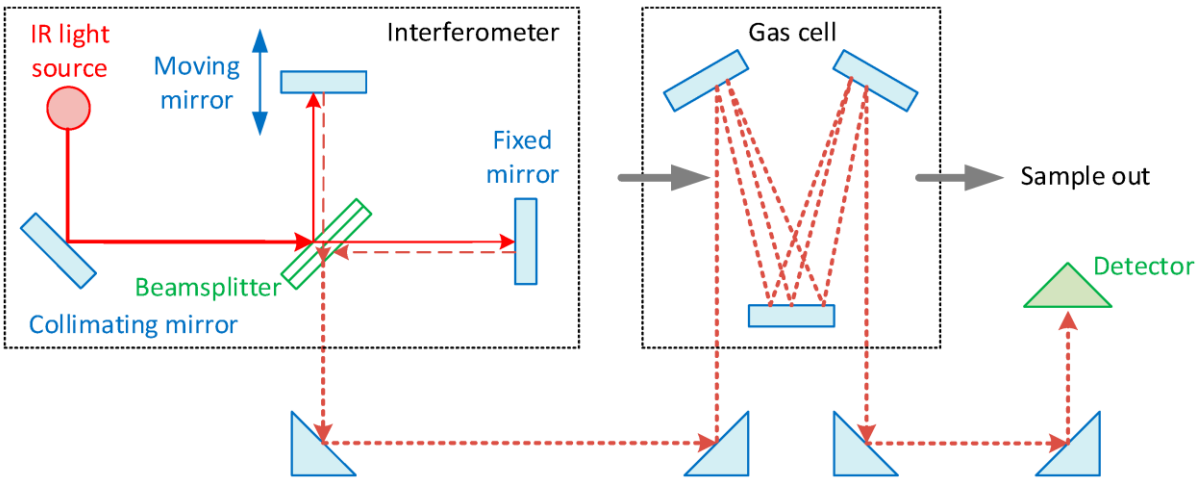

Figure 2.7: Schematic of Fourier transform infrared spectroscopy [32]

Both inorganic and organic compounds can be detected using technique which is non-destructive, Fourier transform infrared spectroscopy. The FTIR setup is shown in the Fig. (2.7). This technique measures the response of sample towards absorption of infrared light. The resulting specimen is a plot with the percentage transmittance on the Y-axis and the

wavenumber, which is the reciprocal of wavelength, on the X-axis. The structures and molecular components are identified by the spectrum's bands. When a light beam passes through a collection of mirrors in FTIR, its various wavelengths collide, either transmitting or absorbing the sample. Infrared radiation raises the energy levels of molecular vibrations. The absorbed wavelengths are specific to specific kinds of chemical bonds and can be used to identify organic metallic compounds both at rest and in their excited vibrational states. A mathematical approach known as the Fourier transform is utilized to measure absorption and convert it into digital data [31].

2.3.4 Scanning electron microscopy (SEM)

A SEM uses an intense, highly focused electron beam to examine the surface microstructure of the material. The sample’s surface structure is analyzed through an electron beam, which interacts with it to produce a variety of signals. The appropriate detectors collect these signals in a raster pattern at each place to produce an image. The electron beam from an electron gun is focused onto a particular area of the sample surface by means of two condenser lenses. As a result, either secondary electrons or backscattered electrons are produced on the sample's surface. These are subsequently picked up and magnified to make an image on the computer screen. When an electron beam strikes a sample, it interacts with the surface in a pear-shaped manner, often extending between one and five micrometers below the surface. Every depth level emits a separate signal. The accelerating voltage can be changed to alter this level [32].

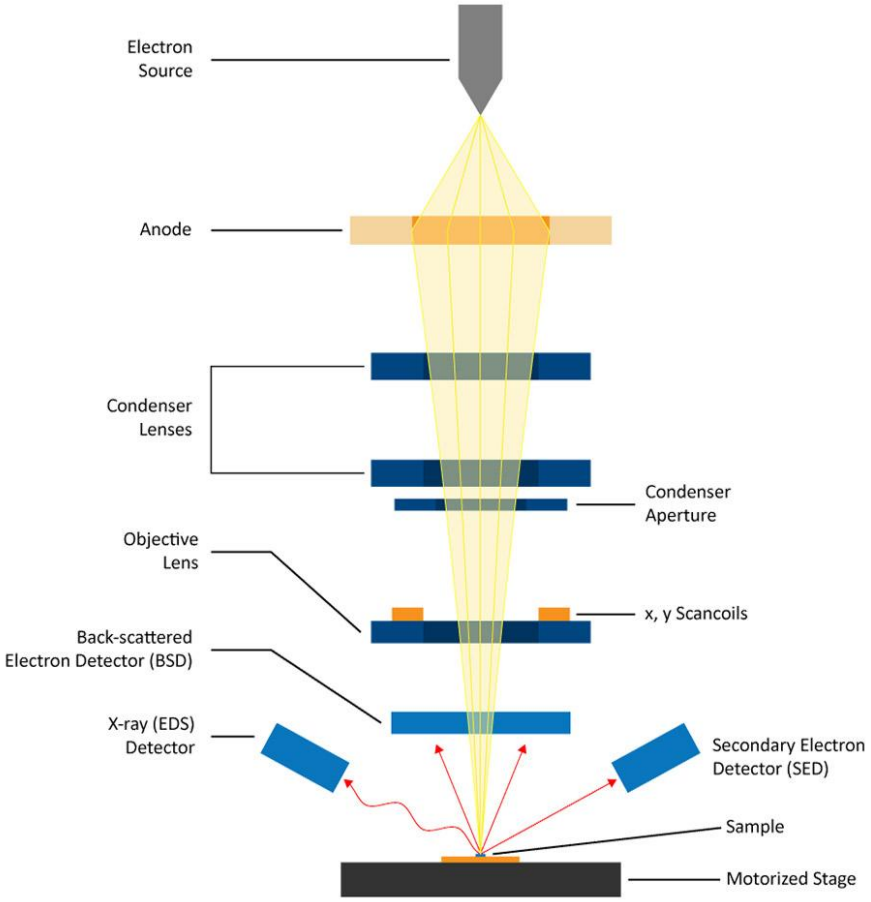

Figure 2.8 Schematic of SEM [33]

2.3.5 Electrochemical characterization

Each component that makes up a supercapacitor has an impact on the device's performance. It is crucial to thoroughly test and examine every component in order to increase its efficiency. Electrochemical impedance spectroscopy, cyclic voltammetry, and galvanostatic charge-discharge are important methods for study and enhancing supercapacitors. Important characteristics including specific capacitance, energy density, and power density are measured with the use of these electrochemical tests and are important for practical SC applications [6].

A) Electrochemical experimental setup to test the electrode supercapacitive performance

A PARASTAT-4000 Potentiostat / Galvanostat (Princeton Applied Research, USA) was used for electrochemical testing. Individual electrodes in non-aqueous electrolytes were studied using a three-electrode setup. In the configuration, the three electrodes were, thin film sample as the working electrode (WE), platinum wire as the counter electrode (CE) and Ag/AgCl as the reference electrode (RE). The size of the working electrode was maintained at 1 cm by 1 cm. Quantifications like as CV and GCD were performed electrochemically using VersaStat Studio 2.10.01 software.

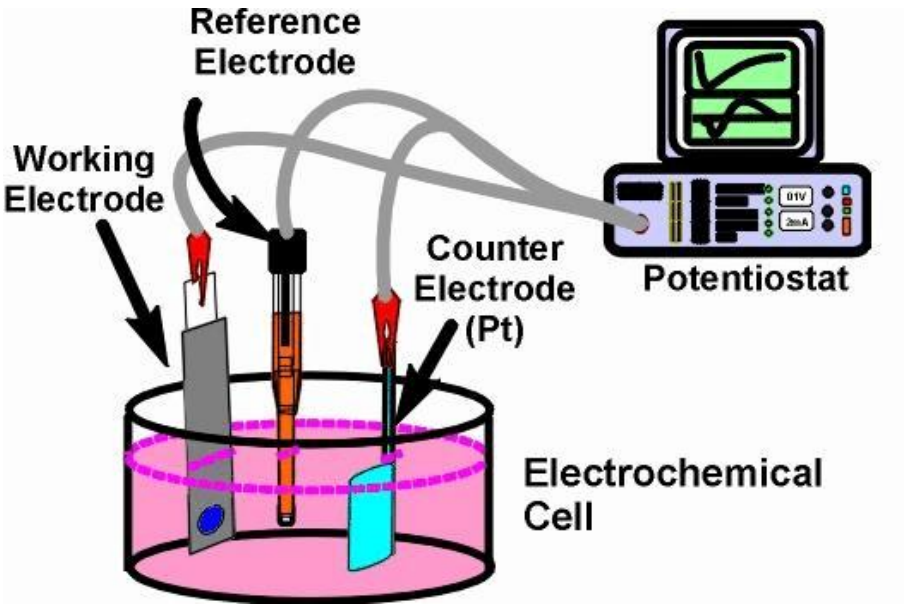

Figure 2.9: Schematic of potentiostat with 3-electrode configuration

B) Cyclic Voltammetry:

cyclic voltammetry (CV) one popular method for examining the electrochemical behavior of electrodes. This technique gradually alters the voltage delivered to the working electrode over time. The working electrode is submerged in an electrolyte solution, and the current between the working and counter electrodes is measured while the potential between

the working and reference electrodes is applied. From a lower value (V_1) to a higher value (V_2) and back to V_1, the voltage is swept between two predetermined boundaries. The scan rate is the speed at which the voltage changes. A larger current is the result of a thinner diffusion layer caused by a quicker scan rate. A typical CV curve for a reversible process is displayed in Fig. 2. The beginning and finishing voltages are V_1 and V_2. I_{PC} and I_{PA} are the corresponding peak currents, whereas V_{PC} and V_{PA} are the voltages at which reduction and oxidation peaks occur. The cathodic current rises and falls during the forward scan as a result of increasing the voltage till the analyte is decreased. The direction of the voltage is inverted at the switching point. An anodic (negative) current is produced as a result of the oxidation of the previously reduced analyte. For reliable findings, selecting the appropriate voltage range (potential window) is crucial as the potential window of supercapacitor depends on the decomposition potential and redox potential of the electrolyte solution [33], [34].

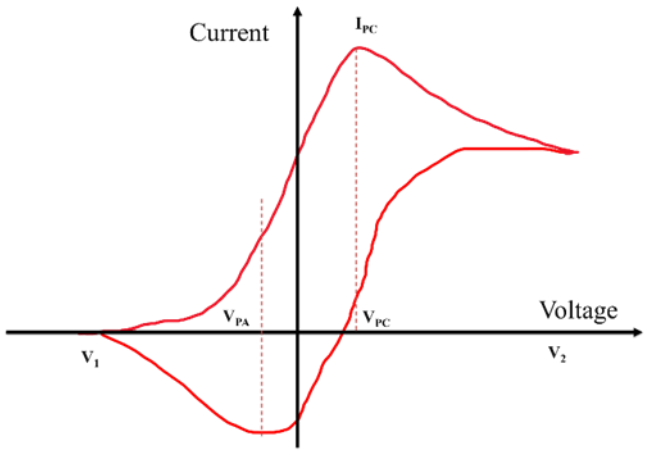

Figure 2.10: CV curve of a reversible single electrode reaction.

Because SCs offer a higher power density than batteries and a significantly higher specific capacitance than conventional capacitors, SCs have gained significant importance in power electronics and high-power applications. As previously mentioned, electric double-layer capacitance (EDLC) and pseudocapacitance are the two primary ways that SC function. While PCs display redox peaks as a result of chemical reactions, EDLCs often display a rectangle on the CV (cyclic voltammetry) graph. The following formula can be used to determine these devices' specific capacitance (Cs):

$$\mathrm{Cs} = \int_i^f \frac{I(v)dv}{m\, v\, \Delta v} \tag{2.4}$$

where, C_S : specific capacitance, ΔV: potential window, m: mass loading and v: scan-rate and the integral from numerator gives the area enclosed by CV curve.

Areal capacitance from CV voltammogram curve is given by following equation (2.5).

$$\text{Areal capacitance} = \frac{Area\ of\ CV\ voltammogram\ curve}{A' \times V \times v} \tag{2.5}$$

where, A'= area of an electrode immersed in electrolyte, V= voltage window and *v* = scan rate.

C) Galvanostatic charge discharge (GCD):

Often referred to as "chronopotentiometry," the galvanostatic charge-discharge (GCD) is very different from the CV in that potential is measured in response to time at constant current. The galvanostatic charge-discharge technique is frequently used to investigate the capacitance, power density, and energy density of various energy storage devices, including SCS, batteries, fuel cells, etc. The following expression is employed to compute the specific capacitance of the electrode connected to the electrochemical storage systems. One of the significant features seen in GCD is ohmic drop, also known as iR drop. The resistance in the electrolyte, electrode, and related interface is the cause. Since iR drop disrupts the potential profile, it should be eliminated or at the very least reduced. Using GCD curves, we have approximated SC properties in this thesis, including specific capacitance (F/g), energy density (Wh/kg), and power density (W/kg). The power density indicates the rate at which the device can supply energy, whereas the energy density shows the ability to perform the task. The following formulas are used to determine these values [35].

$$\text{Specific energy density} = \mathrm{SE} = \frac{1}{2}\frac{CsV^2}{(3.6)} \tag{2.6}$$

$$\text{Specific power density} = \text{SP} = \frac{SE.(3600)}{\Delta t} \quad (2.7)$$

where, C_S is specific capacitance, V is voltage window and Δt is discharge time.

Areal capacitance from galvanostatic charge-discharge (GCD) plot is given by equation (2.7).

$$\text{Areal capacitance} = \frac{Current\ density \times D'}{A' \times (V - V')^2} \quad (2.8)$$

where, A'= area of an electrode immersed in electrolyte, V= voltage window, V'= voltage drop and D'= area under discharge curve.

D) Electrochemical impedance spectroscopy (EIS):

The energy storage system's electrochemical activity can be thoroughly examined using electrochemical impedance spectroscopy. System characteristics can be efficiently assessed by the EIS measurements without being substantially changed. We can calculate the electrochemical system's equivalent series resistance with the aid of EIS. EIS is often carried out under an open circuit voltage situation (0.1 Hz to 100 khz) with a very low amplitude of alternating potential (~ 5 to 10 mv). $Z = Z' + jz''$ is the simple AC resistance of the cell, where Z' and Z'' are the real and imaginary parts of the impedance, respectively. The resistive behavior is represented by the real part, while the capacitive and inductive behavior are represented by the imaginary part. The Nyquist plot is the most often used method for analysing EIS data. Plotting imaginary impedance (Z'') against real impedance (Z') is what it is. Three regions of frequency high, medium and low. Regions can be identified in the magnified EIS plot view. Together, the semicircular region at high frequencies and the electrode resistance at extremely up to the semicircle's beginning represent the system's internal resistance (R_S). At high frequencies, the semicircular region represents the bulk electrolyte resistance. The diffusion process is represented by a line inclined at about 45^o at medium frequency, whereas the ideal capacitive ion diffusion is represented by a line inclined at 90^o. The change transmission mechanism and diffusion of ions into the electrode's pores

are the sources of the interfacial charge transfer resistance (R_{CT}). Therefore, the corresponding equivalent circuits present a clear overview of the various mechanisms involved in energy storage. By measuring the relaxation time constant (τ), it is simple to tell the difference between the capacitive and resistive behavior of the SCs. The relaxation time constant can be assessed by plotting imaginary capacitance (C″) against frequency (f).

$$\tau = \frac{1}{f} \tag{2.9}$$

Where,

$$C'' = \frac{Z'}{2\pi f |z|} \tag{2.10}$$

where f denotes the characteristic frequency and Z" and Z' denotes the complex impedance and real impedance component respectively.

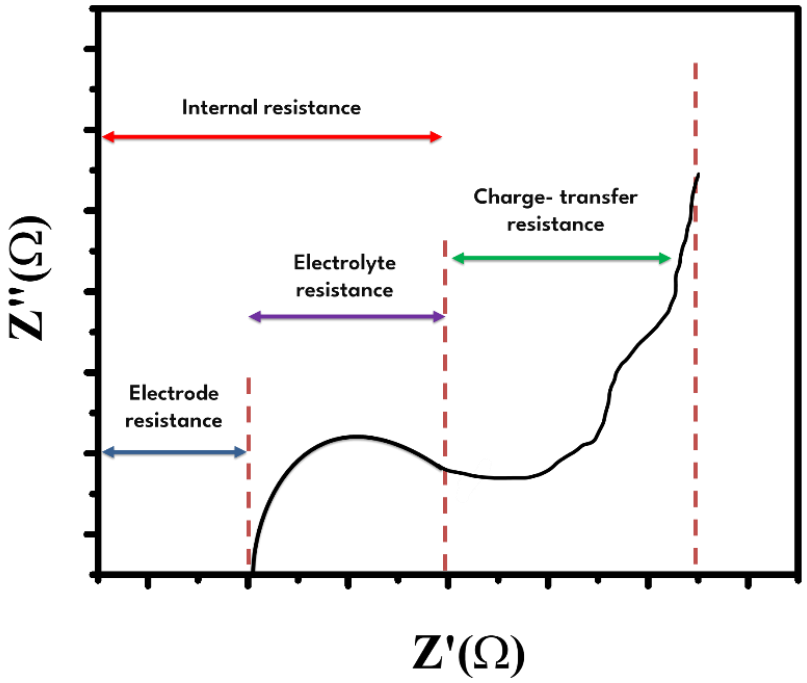

Figure 2.11 Electrochemical impedance spectroscopy

High supercapacitive activities, which are linked to high-power transport, are caused by low relaxation times. Bode plots can be used to study the relationship between phase angle and frequency, and by figuring out the frequency corresponding to 45°, we can estimate the relaxation time constant (τ) with the help of equation (2.7).

CHAPTER III

VANADIUM SELENIUM OXIDE BASED THIN FILM BY SILAR METHOD FOR SUPERCAPACITOR APPLICATION

3.1 Introduction

The present-day research in the field supercapacitor is oriented in producing cost effective, thin, lighter and flexible ultracapacitors. We have used simple, easy and less expensive method of deposition. In this work we have deposited thin film of vanadium selenium oxide based thin film by successive ionic layer adsorption and reaction method for application in supercapacitor. This chapter also includes the structural and electrochemical study of V-Se-O based electrode material.

3.2 Experimental studies

3.2.1 Materials

Vanadyl sulfate ($VOSO_4$) of LOBA Chemie company with 99.9% purity, selenium powder of SDFCL company with 99.9% purity, sodium sulfite (Na_2SO_3) of Merk company with 98% purity, Hydrazine (N_2H_4), $LiClO_4$ and $NaClO_4$ of Sigma Aldrich company with 95% and 98% purity respectively and acetonitrile (CH_3CN) of LOBA Chemie company with 99% purity were used for the synthesis of vanadium selenium oxide based thin film. Stainless steel of grade 304 and thickness 0.01 mm was used as substrate.

3.2.2 Synthesis of vanadium selenium oxide based thin film

V-Se-O based a thin film was deposited over the SS substrate by simple and cost-effective, successive ionic layer adsorption and reaction method. Vanadyl sulphate ($VOSO_4$) was used as cationic precursor and sodium selenosulfate (Na_2SeSO_3) was used as an anionic precursor.

3.2.2 (a) Substate selection and cleaning process

In the creation of supercapacitor devices, the conducting substrate is essential. It must be flexible, lightweight, reasonably priced, easily accessible, and have a low angle of contact with the deposited layer in order to guarantee good adherence. In the production of supercapacitors, nickel foam, copper, titanium, stainless steel, and other metals are frequently utilized as substrate materials. Because of its affordability, high conductivity, and ease of access, we decided to use stainless steel in our investigation to make it cost effective. Nevertheless, surface impurities found on substrates can obstruct thin film nucleation and growth during deposition. Consequently, it is crucial to thoroughly clean the substrate. A uniform thin coating is formed as a result of proper cleaning, which also provides active nucleation sites and lowers contaminants. The following steps are included in the stainless-steel (SS) substrate cleaning process [36].

The steps involved in substrate cleaning:

1. To obtain the uniform film and remove the adhered impurity particles, the SS of dimensions 3.5 cm × 5 cm was first rubbed with sandpaper-220.
2. Cleaning of the stainless steel was carried out with labolene followed by double-distilled water.
3. The SS substrate was ultrasonicated for 30 mins (the used beaker is cleaned with acid first, then labolene and lastly with DDW).
4. Then the substrate was rinsed with DDW and dried completely.

3.2.2 (b) Preparation of the precursor

Preparation of cationic precursor: Vanadyl sulphate ($VOSO_4$) solution of 0.1M was used as the cationic solution. For this 0.8150 g of $VOSO_4$ salt was dissolved in 50 ml of DDW with the help of magnetic stirrer.

Preparation of anionic precursor: Sodium selenosulfate (Na_2SeSO_3) in DDW of 25:25 ratio with addition of 4 ml of hydrazine was used as the anionic precursor. Na_2SeSO_3 was prepared by dissolving 15 g of sodium sulfite (Na_2SO_3) and 5 g of selenium (Se) powder in 200 ml

DDW and refluxed at temperature of 90°C for 9hr [37]. Then the solution was filtered to extract sodium selenosulfate solution using Whatman filter paper. As prepared solution of 25 ml was mixed with 25 ml of DDW with 4 ml hydrazine (N_2H_4) and used as the anionic precursor.

3.2.3 Thin film of V-Se-O based on SS by SILAR method.

- **Adsorption**

  Cleaned SS substrate was immersed in 50 ml solution of 0.1 M $VOSO_4$ for 20 s where VO^{2+} ions are adhered on the surface of SS substrate.

- **Rinsing I**

  In this step Substrate was immersed in 50 ml of DDW for 5 s to remove VO^{2+} ions which were loosely adhered on the substrate.

- **Reaction**

  The subsequent step involved immersing the substrate in the anionic precursor for 20 s. where selenium anions (Se^{2-}) from Na_2SeSO_3 solution were reacted with pre-adsorbed VO^{2+} ions to form $V_2(Se_2O_9)$.

- **Rinsing II**

  Then it rinsed with double distilled water by immersing it in 50 ml DDW beaker for 5 s to get rid of any unreacted ion and loosely attached particles. This process was repeated for 75 cycles.

Table 3.1: Preparative parameters for the deposition of $V_2(Se_2O_9)$ thin film.

Breaker No.	Precursor solution	Dipping time (s)	Temperature (°C)
I	0.1 M $VOSO_4$	20	28
II	DDW	5	
III	$Na_2SeSO_3 + N_2H_4$	20	
IV	DDW	5	

3.3 Characterizations

The crystal structure of as synthesized $V_2(Se_2O_9)$ was studied with the help of Ultima IV, Rigaku Corporation, Japan; X-ray diffractometer using Cu-K_α radiation having wavelength λ= 1.5406 Å and range of 2θ was 10° to 90°. Wettability of surface was studied by measuring contact angle using digital camera. Fourier transform infrared spectroscopy (FTIR) study were carried out in 4000 cm^{-1} to 500 cm^{-1} to analyze chemical bonds. The electrochemical studies such as cyclic voltammetry (CV), electrochemical impedance spectroscopy (EIS) and galvanostatic charge-discharge (GCD) of electrodes were carried out with the help of PARASTAT-4000 potentiostat/galvanostat (Princeton Applied Research, USA), coupled with Versa-stat studio 2.10.01 software. The electrochemical performance was investigated in three electrodes configuration, with Ag/AgCl as reference electrode (RE), SS/$V_2(Se_2O_9)$ as working electrode (WE) and Pt wire as counter electrode (CE).

3.4 Results and discussion

3.4.1 Surface wettability study

Minimum observed contact angle increases the surface wettability which results in more interaction between the electrode and electrolyte. To plunge the DDW drop onto SS and SS/$V_2(Se_2O_9)$, a micropipette was used. Image was captured by the digital camera. As shown in fig 3.2, the contact angle of SS with water was measured as 52.54°, which is lesser than 90°

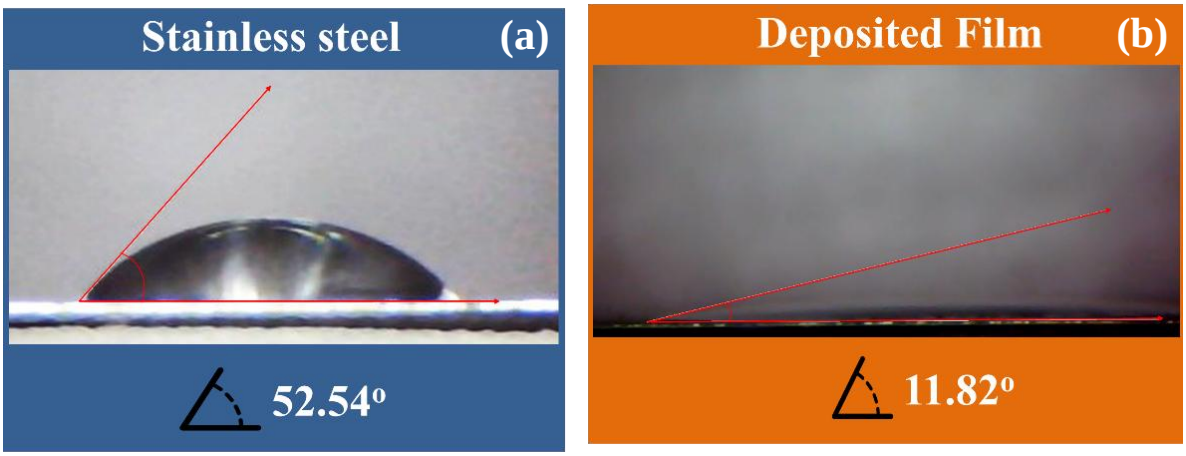

Figure 3.1: Contact angle measurements of (a) SS with DDW, (b) SS/ V2(Se2O9) with DDW

[26]. The deposition of $V_2(Se_2O_9)$ reduces contact angle to 11.82° enabling its suitability for electrode material hydrophilic towards supercapacitor applications.

3.4.2 X-ray diffraction analysis (XRD)

The structural identification of V-Se-O based thin film was studied by X-ray diffraction. Fig. (3.2) shows the XRD patterns of $V_2(Se_2O_9)$ in powder form. The non-intense pattern exhibits nanocrystalline nature of obtained material. The obtained data was compared with JCPDS 89-0386 card. The sample of $V_2(Se_2O_9)$ material shows one major peaks at 2θ values of 28.00° corresponds (h k l) plane along (0 3 1). Whereas two minor peaks at 50.86° and

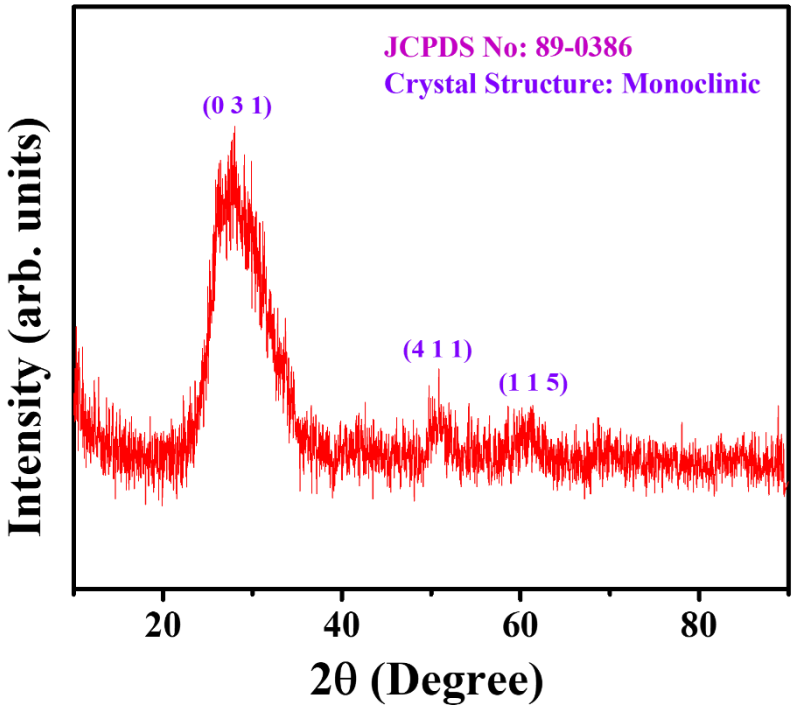

Figure 3.2: XRD pattern of $V_2(Se_2O_9)$ sample

60.71° represents (4 1 1) and (1 1 5) planes with monoclinic crystal structure respectively. The Debye–Scherrer formula was used to calculate the average crystallite size of the deposited films, which was found to be 1.33 nm.

3.4.3 Fourier transform infrared spectroscopy (FTIR)

To study bonding in $V_2(Se_2O_9)$ FTIR study was performed and in Fig. 3.3. The characteristic peaks of $V_2(Se_2O_9)$ were observed at 550.58, 763.67, 998.46, 1136.35, 1625.69,

and 3425.44 cm^{-1}. The maximum absorption is corresponding to Se-O terminal stretching corresponding to wavenumber 550.58 cm^{-1}, 763.67 cm^{-1} is corresponding to deformation of

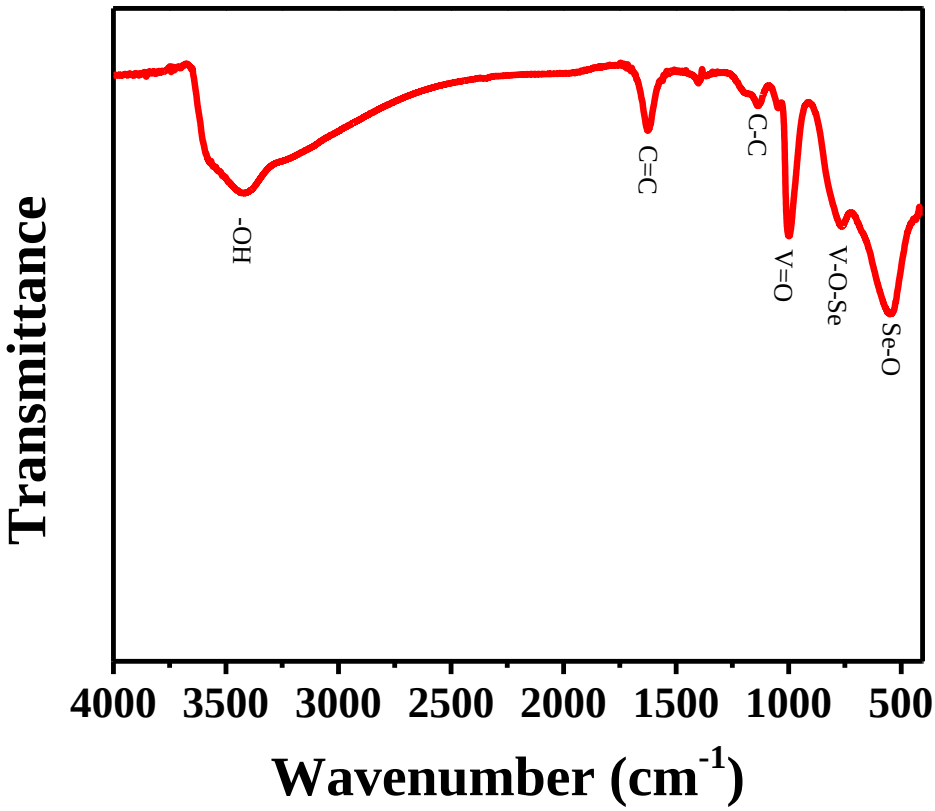

Figure 3.3: Fourier transform infrared spectroscopy of $V_2(Se_2O_9)$ sample

V-O-Se previously reported by Muhammad Munir Sajid et al. [38]. 998.46 cm^{-1} which correspond to the stretching of V=O reported by Yong Cheol Hong et al.[39]. 1136.35 cm^{-1} and 1625.698 cm^{-1} are corresponding to the C-C and C=C stretching and their present is due to atmospheric carbon. The peak on extreme end that is 3425 cm^{-1} is corresponding to -OH stretching which shows absorption of water.

3.4.4 Surface morphological study

The morphological study has been carried out for SS/$V_2(Se_2O_9)$ through SEM images for 50, 75 and 100 number of SILAR cycles and their corresponding SEM images are shown as (a), (b) and (c), respectively with same magnification 1kX. Here the crowdedness of material increased as number of SILAR cycles increased from 50 to 100, that shows higher mass loading with respect to increase in SILAR cycles. From these images, it was concluded that deposition is uniform throughout the thin film. Fig. 3.4 (d) and (e) are of 100 kX

magnification of 75 and 100 SILAR cycles deposited film respectively. The particles size is ranging from 45 nm to 190 nm denoted as (1) and (2) respectively in Fig. 3.4 (e). As number of cycles increased, the particle size increased may reduce electrochemical active sites corresponding to 100 SILAR cycles. The morphology is nano-spherical in nature.

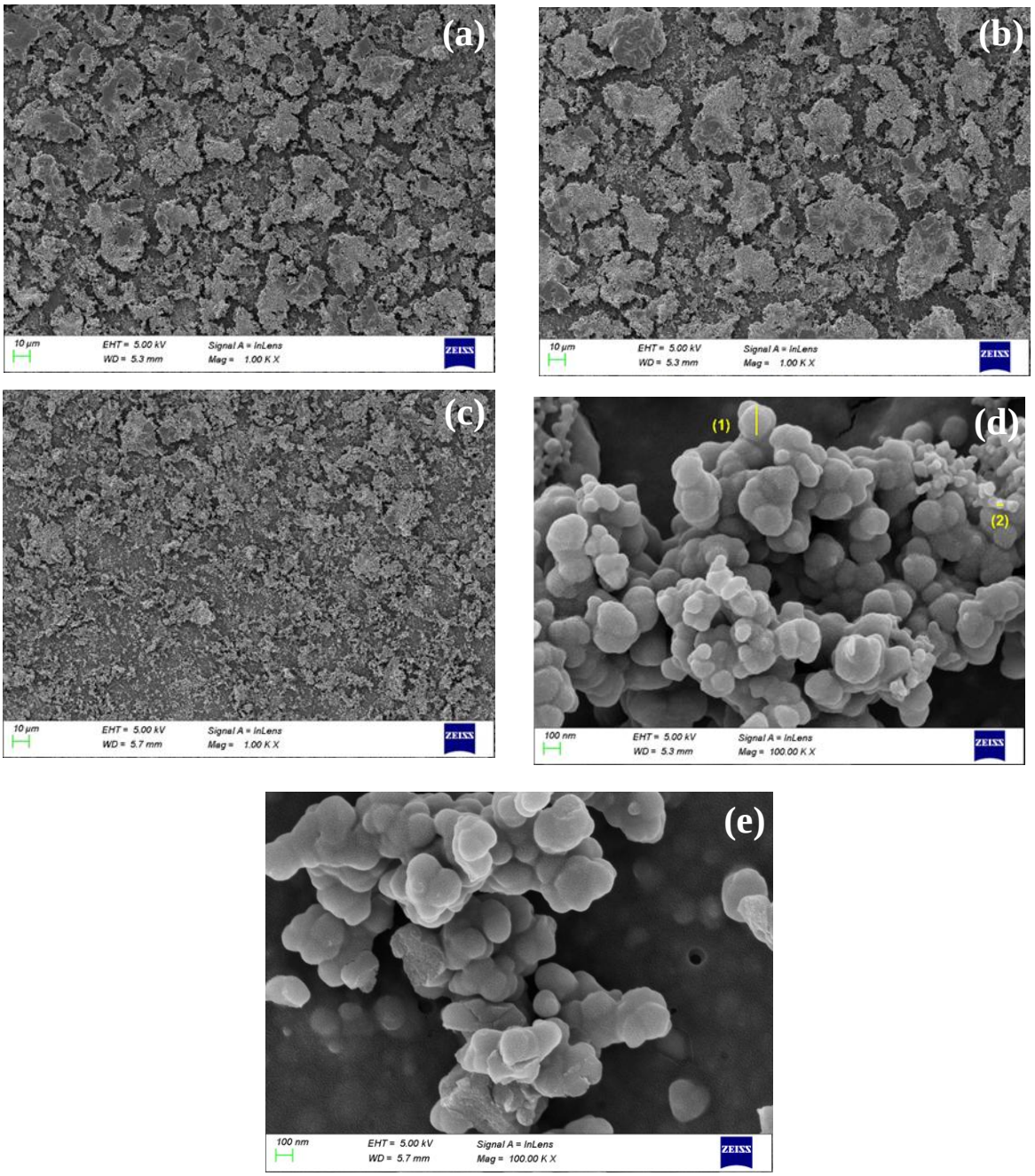

Figure 3.4: SEM images of $V_2(Se_2O_9)$ for (a) 50, (b)75 and (c)100 SILAR cycles and fig. (d) and (e) shows images at 100 nm for 75 and 100 SILAR cycles respectively.

3.4.5 Supercapacitor studies of electrode (Electrochemical studies)

1 **Electrolyte optimization:** To examine the electrochemical performance of SS/$V_2(Se_2O_9)$, cyclic voltammetry (CV) tests were performed. The Fig. 3.5 (a) shows the CV curve of SS/ $V_2(Se_2O_9)$ in different electrolyte.

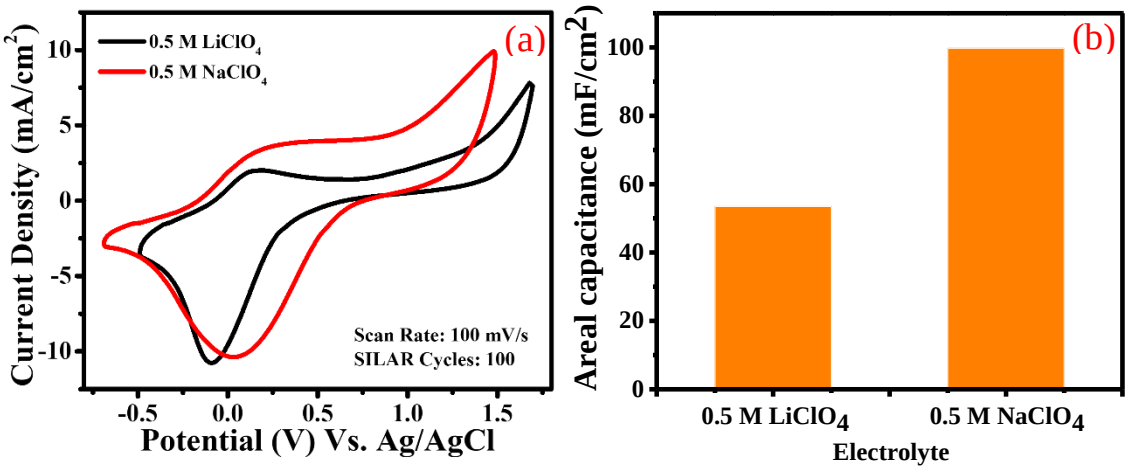

Figure 3.5: (a) CV curves of in $LiClO_4$ and $NaClO_4$ electrolytes, (b) Areal capacitance for $LiClO_4$ and $NaClO_4$ electrolytes

The CV curves for different electrolytes of fixed concentration (0.5 M) and scan rate (100 mV/s) were studied to find the most suitable electrolyte, which gives high specific capacitance. Thus, for optimization of electrolyte for supercapacitor electrode SS/$V_2(Se_2O_9)$, non-aqueous solutions of $LiClO_4$ and $NaClO_4$ in acetonitrile was used. Among these, the solution of 0.5M $NaClO_4$ shows the highest areal capacitance with 99.75 mF/cm^2 as shown in Fig. 3.5 (a) and (b). Throughout the measurements, the areal capacitance calculated from CV voltammogram was by using equation (2.5) from chapter II.

2 **Concentration:** Further optimization is done for different concentrations of $NaClO_4$, shown in Fig. 3.6 (a) and (b). The areal capacitance was highest in 0.5 M $NaClO_4$ solution. This may be because of an increase in the concentration results in an increase in the number of ions in electrolytes increases which leads to more current, which results in a

large area curve [21], [33], [34]..

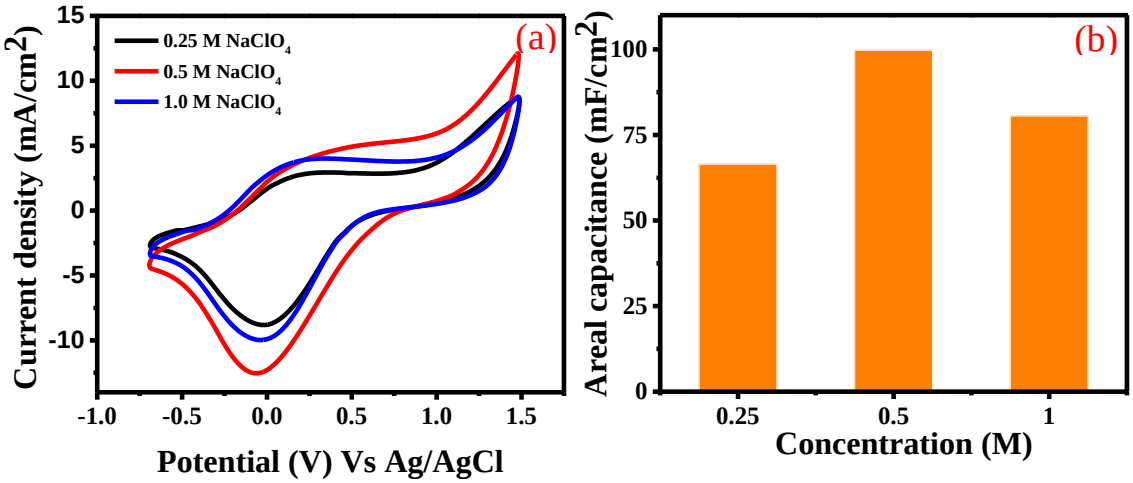

Figure 3.6: a) CV curves with different concentration of $NaClO_4$, (b) Areal capacitance vs concentration.

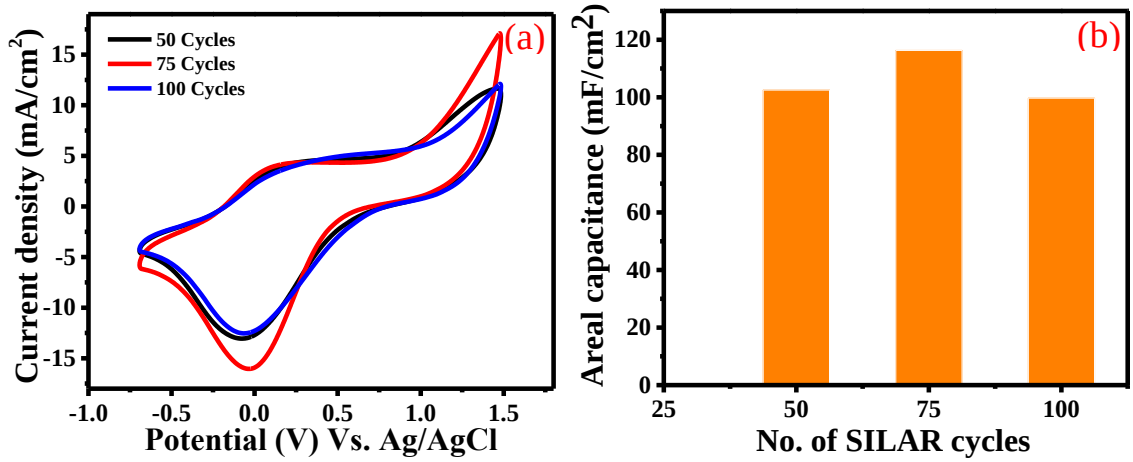

Figure 3.7: (a) CV curves with different SILAR cycles, (b) Areal capacitance at different SILAR cycles

3. Effect of number of SILAR cycles: CV of SS/ $V_2(Se_2O_9)$ with different SILAR cycles is also performed to optimize the SILAR cycles, which shown maximum areal capacitance with value of 116.3 mF/cm2 for the electrode deposited with 75 SILAR cycles, as shown in Fig. 3.7 (a) and (b). With increase in the number of SILAR cycles, the mass loading is increased which in turn enhances the charge storage capabilities. Also, there might be an increase in

surface area for an optimum number of SILAR cycles. Further increase in the SILAR cycles from 75 to 100 results in the increased particle size, thereby minimizing the electrochemical active sites, which results in reduced capacitances.

4. Effect of scan rate: Cyclic voltammetry of SS/$V_2(Se_2O_9)$, electrode at different scan rates of 100, 75, 50, 25, 10, 5, and 2 mV/s in the electrolyte solution of 0.5 M $NaClO_4$ with constant potential window (PW) of 2.2 V (-0.7 to 1.5 V) and are shown in Fig. 3.8 (a) and (b).

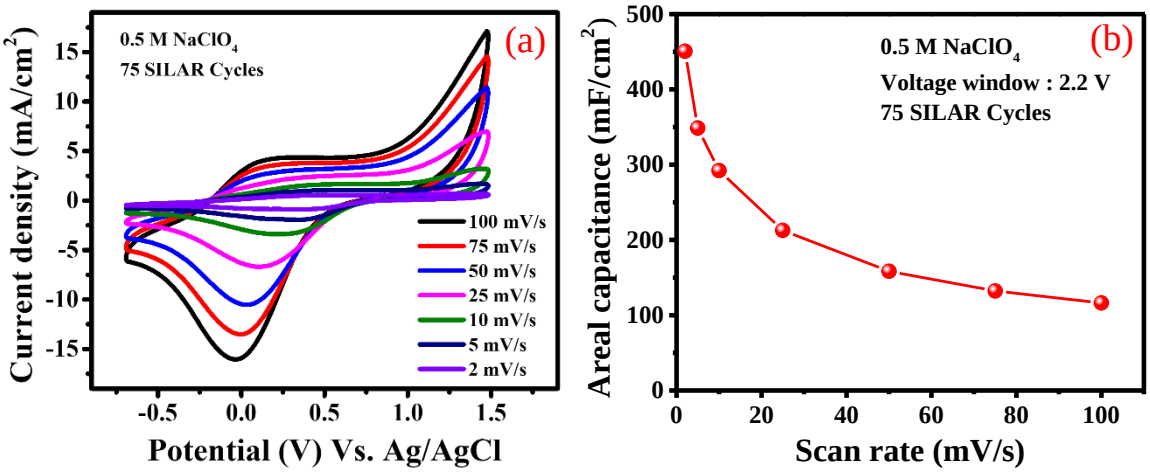

Figure 3.8: (a) CV plots at different scan rates, (b) Areal capacitance at different scan rate

Oxidation and reduction peaks observed in the CV voltammogram Indicates pseudocapacitive behavior of the $V_2(Se_2O_9)$, electrode material. The shape of the curve remains similar at different scan rates from 2 to 100 mV/s, which shows good electrochemical reversibility. The $V_2(Se_2O_9)$ exhibit higher areal capacitance of 450.72 mF/cm^2 at scan rate 2 mV/s, this is because sufficient time for electrolyte ions to interact with electrolyte in electrochemical process. With increase in scan rate the areal capacitance decreased and reached 116.35 mF/cm^2 at 100 mV/s as shown in Fig. 3.6 (a) and (b).

5. Cyclic stability: There is capacitive retention of 83.86% for SS/$V_2(Se_2O_9)$ working electrode in 0.5M $NaClO_4$ in acetonitrile after 1000 charge-discharge cycles as shown in Fig.3.10 (a) and (b). With increase in the number of cycles, the oxidation and reduction peaks reduced due to the material degradation, resulting in reduced capacitive retention.

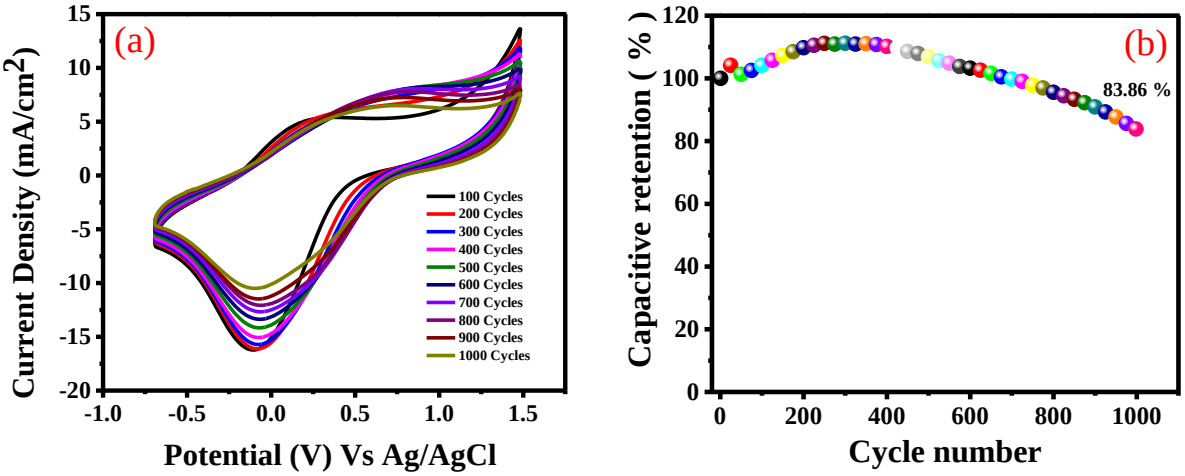

Figure 3.10: (a) CV plots at different number of cycles, (b) Capacitance retention vs number of cycles.

6. Effect of current density: An efficient way to investigate the supercapacitor performance of the electrode material is GCD. The Fig 3.9 (a) and (b) shows a comparison of GCD curves with different constant current densities from 1 to 4 mA/cm^2 in the potential window, ranging from -0.7 V to 1.5 V.

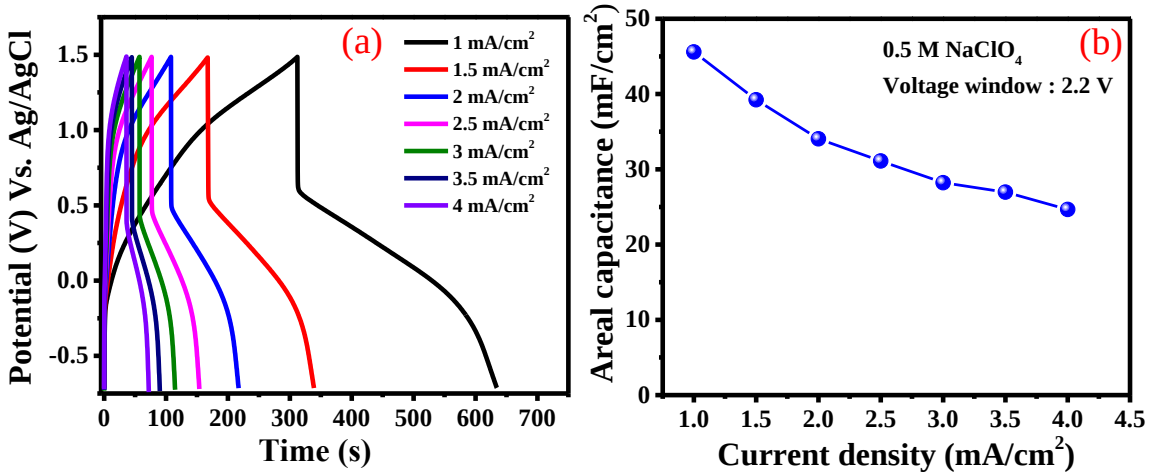

Figure 3.9: (a) GCD plots at different current densities, (b) Areal capacitance vs current densities

The GCD curves of the SS/ $V_2(Se_2O_9)$ showed rapid voltage drop of approximately

1V because of the intrinsic resistive behavior of the material [35]. The maximum areal capacitance of 45.60 mF/cm^2 was obtained at the current density 1 mA/cm^2 and reaches to 24.67 mF/cm^2 at 4 mA/cm^2. Throughout the measurements, the areal capacitance calculated from GCD curve was by using equation (2.5) from chapter II.

7. **Electrochemical impedance spectroscopy (EIS):** Electrical conductivity, diffusion of ions, the cause of charge storage behavior, the charge transfer process in SCs are all examined with the help of EIS. The graph plotted between imaginary impedance (Z″) and real impedance (Z′) is called Nyquist plot, which is recorded in the range of 0.1 Hz to 100 kHz. The Nyquist plot data were fitted to a corresponding equivalent circuit of R(Q(R(CW))) with the help of software Z-simpwin to simulate. The fitted circuit comprises solution resistance (R_S), double layer capacitance (C_{DL}), constant phase element (CPE), charge-transfer resistance (R_{CT}) and Warburg impedance (W). The observed partial semicircle indicates the charge-transfer resistance (R_{CT}) associated with the reversible Faradaic redox process during electrochemical charge-discharge activities. The values of R_S and R_{CT} are 4.27 Ω.cm$^{-2,}$ and 27.47 Ω.cm^{-2} and respectively. The linear segment observed in the region of low-frequency represents limit of mass transport.

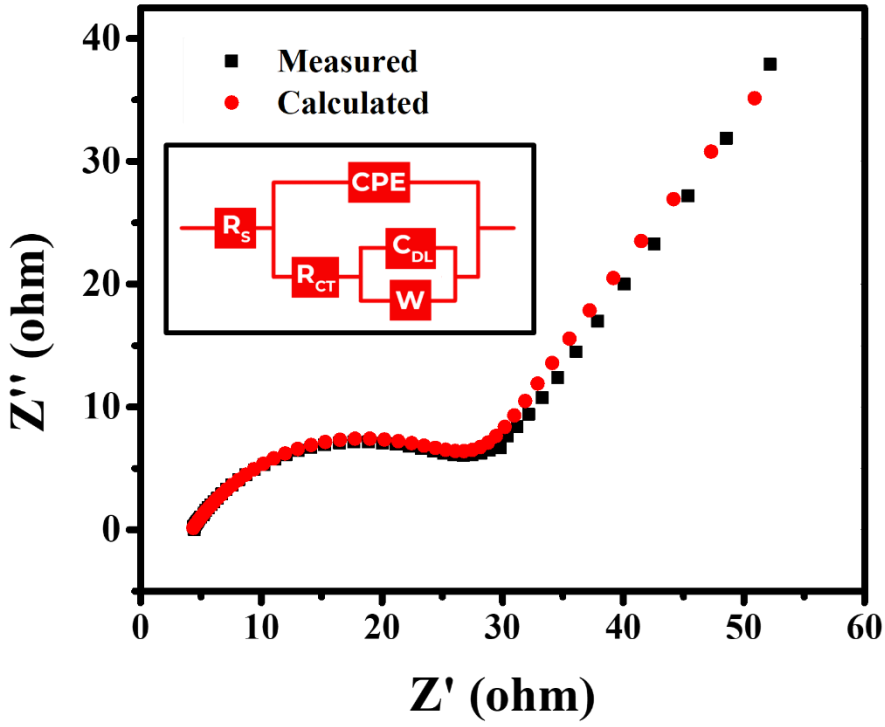

Figure 3.11: Nyquist plot and inset shows equivalent circuit

Table 3.2: Electrochemical impedance spectroscopy measurements

Sr. No.	Element	Impedance (Ω/cm^2)
1	Solution resistance	4.27
2	Charge-transfer resistance	27.47
3	Warburg impedance	0.02

In EIS experiment, the capacitor frequently does not behave ideally, they exhibit behavior similar to a constant phase element. The constant phase element is in parallel with (R(CW)). The slope of the straight line in the region lower frequency is represented by Warburg impedance element, which is consequence of dependency of diffusion of ions on frequency.

CHAPTER IV

SUMMARY AND CONCLUSIONS

4.1 Introduction

When it comes to do synthesis of nanomaterials, thin film deposition methods are very successful. The SILAR (Successive Ionic Layer Adsorption and Reaction) method, a straightforward and inexpensive technology, was used in this study to develop vanadium selenium oxide ($V_2(Se_2O_9)$), thin films on SS. To improve the performance of deposited films for SCs applications, different electrolytes, concentrations, and variation in number of SILAR cycle have been optimized. The four chapters that make up the complete thesis are briefly outlined here.

1. **Chapter I:**

   In this chapter, different energy storage technologies are introduced and their salient characteristics are compared. Supercapacitors are the main focus because of their intermediate energy density and high-power density. A tabular overview of previous studies on vanadium selenide and vanadium selenide oxides is also provided.

2. **Chapter II:**

   The theoretical framework of thin film deposition and different methods of material characterization are covered in this chapter. It describes how thin films are categorized. The SILAR method's foundations, preparation requirements, and advantages. Additionally covered are characterization methods including surface wettability, XRD analysis, SEM analysis, FTIR analysis, cyclic voltammetry (CV), galvanostatic charge-discharge (GCD) and EIS.

3. **Chapter III:**

   The $V_2(Se_2O_9)$ electrode's synthesis, analysis, and operation in a liquid electrolyte-based device are the main topics of this chapter. The SILAR method was used to prepare the electrode. XRD was used to investigate structural characteristics, SEM was used to study surface architecture, FTIR was used to analyze bonds and a variety of methods particularly EIS, CV and GCD were employed to assess electrochemical behavior.

4.1.1 Deposition of the $V_2(Se_2O_9)$ thin film.

There is no report on synthesis of $V_2(Se_2O_9)$ by SILAR method. The optimized preparative parameters are mentioned Table 4.1. The important benefit of deposition by SILAR is cost-effectiveness due to not requirement of sophisticated instrument while carrying out deposition, which gives an edge over other methods in term of synthesizing cost.

Table 4.1: Parameters of preparation for the deposition of $V_2(Se_2O_9)$ thin film.

Breaker No.	Precursor solution	Dipping time (s)	Temperature (°C)
I	0.1 M $VOSO_4$	20	28
II	DDW	5	
III	$Na_2SeSO_3 + N_2H_4$	20	
IV	DDW	5	

4.1.2 Characterizations of thin film

4.1.2 (a) Surface wettability

The considerable reduction in contact angle between water and SS/$V_2(Se_2O_9)$ from 52.54° to 11.82° as shown in Table 4.2 clearly indicates the hydrophilic nature, but consideration of reaction with an electrolyte while carrying out the electrochemical study is very important in case of an aqueous electrolyte.

Table 4.2 Contact angle experiment

Sr. No	Material	Solvent	Contact angle (degree)
1	SS	DDW	52.54^o
2	SS/$V_2(Se_2O_9)$	DDW	11.82^o

4.1.3 (b) X-ray Diffraction (XRD)

The JCPDS 89-0386 card was used to compare the acquired data. The crystal structure is monoclinic. The one significant peak in the $V_2(Se_2O_9)$ at 2θ values of 28.00° and two minor peaks at 50.86° and 60.71° corresponding to (0 3 1), (4 1 1) and (1 1 5) respectively. According to the Debye Scherrer formula, the average crystallite size is 1.33 nm.

Table 4.3 XRD peaks and respective planes of $V_2(Se_2O_9)$.

Sr. No	Peaks (2θ) (degree)	(h k l) planes
1	28.00	(0 3 1)
2	50.87	(4 1 1)
3	60.71	(1 1 5)

4.1.2 (c) Fourier transform infrared spectroscopy (FTIR)

The resulting FTIR absorption spectra are displayed in table 4.4. At 550.58 cm^{-1}, 763.67 cm^{-1}, 998.46 cm^{-1}, 1136.35 cm^{-1}, 1625.698 cm^{-1}, and 3425.44 cm^{-1}. The distinctive peaks of $V_2(Se_2O_9)$ were detected. Maximum absorption corresponds to Se-O terminal stretch at wavenumber 550.58 cm^{-1}, deformation of V-O-Se at wavenumber 763.67 cm^{-1}, and V=O stretching at wavenumber 998.46 cm^{-1}. The C-C and C=C stretching are represented by 1136.35 cm^{-1} and 1625.698 cm^{-1}, respectively, and their current state is caused by atmospheric carbon. 3425 cm^{-1} is corresponding to stretching of hydroxyl, showing absorption of water.

Table 4.4 Fourier transform infrared spectroscopy analysis

Sr. No	Bond type	Wavenumber (cm^{-1})
1	Se-O	550.58
2	Se-O-Se	763.67

3	V=O	998.46
4	C-C	1136.35
5	C=C	1625.70
6	-OH	3425.44

4.1.2 (d) SEM Analysis

In SEM images analysis nano-spherical morphology is there with nanospheres ranging from 45-90 nm. Increased number of SILAR cycles lead to more agglomeration which increased the particle size resulting in reduced electrochemical active sites.

4.1.2 (e) Electrochemical studies

1. SILAR cycles variation

In acetonitrile $NaClO_4$ showed a greater cyclic voltammetry (CV) curve area than $LiClO_4$. This is may be because of solvation. Na^+ ions are less strongly solvated in acetonitrile and are bigger than Li^+ ions. Because of this reduced solvation, Na^+ can pass through the solvent more readily and can access electrode surface easily. On the other hand, Li^+ ions are slowed down and find it more difficult due to the tight solvation. For $NaClO_4$ in acetonitrile an organic electrolyte showed maximum areal capacitance for 0.5 M concentration.

Table 4.5 Areal capacitance of $V_2(Se_2O_9)$ in different electrolytes at 100mV/s

Sr. No	Electrolyte	Areal Capacitance (mF/cm^2)
1	0.5 M $LiClO_4$	53.49
2	0.5 M $NaClO_4$	99.75

Table 4.6: Areal Capacitance of $V_2(Se_2O_9)$ in $NaClO_4$ at different concentrations at 100 mV/s.

Sr. No	Concentration (M)	Areal Capacitance (mF/cm^2)
1	0.25	66.44
2	0.5	99.74
3	1.0	80.51

2. SILAR cycles variation

For 75 SILAR cycles maximum areal capacitance recorded. The reason is as seen from SEM images more surface area is for 75 SILAR cycles due to less agglomeration as compared to 100 SILAR cycles and for 50 SILAR cycles material is less, so optimum values obtained for 75 SILAR cycles.

Table 4.7 Areal capacitance of $V_2(Se_2O_9)$ deposited with different SILAR cycles at 100 mV/s.

Sr. No	SILAR Cycle	Areal Capacitance (mF/cm^2)
1	50	102.5
2	75	116.3
3	100	99.7

3. Scan rate variation

As we increase the scan rate ions have a reduced interaction time with the electrode material. so increasing scan rate leads to decrease in areal capacitance as shown in table 4.8. Interaction time of an ions with an electrode material is modulated due to change in scan rate.

Table 4.8 Areal capacitance of $V_2(Se_2O_9)$ with different scan rate.

Sr. No	Scan Rate (mV/s)	Areal Capacitance (mF/cm^2)
1	100	116.35
2	75	132.19
3	50	158.43
4	25	212.64
5	10	292.09
6	5	348.56
7	2	450.72

4. Effect of current density

Because ions have less time to reach all of the electrode's active sites, capacitance drops as current density rises. Higher capacitance is the result of ions being capable to fully enter the pores and store more charge at low current. Only the outside surface is utilized at high current, which lowers capacitance and charge storage.

Table 4.9 Areal capacitance of $V_2(Se_2O_9)$ at different current densities.

Sr. No	Current density (mA/cm^2)	Areal Capacitance (mF/cm^2)
1	1	45.59
2	1.5	39.24
3	2	34.05
4	2.5	31.10
5	3	28.22
6	3.5	26.97

7	4	24.67

5. Cyclic stability

The capacitive retention of 83.86% after 1000 charge discharge cycles has been found, mainly due to reaction of electrode material with an electrolyte after few 100s of charge-discharge cycles.

6. EIS study

R(Q(R(CW)) is the analogous circuit to which the Nyquist plot is fitted. R_{CT} and R_S have respective values of 27.47 $\Omega.cm^{-2}$ and 4.27 $\Omega.cm^{-2}$. $R_{CT} > R_S$ this shows good ionic conductivity of the electrolyte. A high R_{CT} suggests slow charge-transfer, meaning the electrode surface is not efficient in facilitating the redox reactions.

4.2 Conclusions

A simple and economical SILAR deposition method was used to synthesize the $V_2(Se_2O_9)$ thin film. Working potential window of electrode has been observed was 2.2V (-0.7 V to 1.5 V). The GCD investigations demonstrate a maximum capacitance of 45.59 mF/cm^2 at 1 mA/cm^2 in the potential range of -0.7 V to 1.5 V, while the electrochemical CV studies demonstrate a maximum areal capacitance of 450.72 mF/cm^2 at scan rate 2 mV/s. There is 16.94% of a considerable drop in the ability to maintain capacitance after 1000 repeated charge-discharge cycles.

4.3 Future scope

This study focuses on the synthesis and supercapacitor applications of vanadium selenium oxide by SILAR method which is not reported by anyone with SILAR method. Solid state device study can be more useful in case of this material. Future work can be proposed on synthesis of metal selenide electrode for the fabrication of cost effective, flexible and more efficient supercapacitors and commercialization of prepared supercapacitors is also a one of the challenging works which need to be achieved.

References

[1] N. McIlwaine *et al.*, “A state-of-the-art techno-economic review of distributed and embedded energy storage for energy systems,” Aug. 15, 2021, *Elsevier Ltd*. doi: 10.1016/j.energy.2021.120461.

[2] W. Raza *et al.*, “Recent advancements in supercapacitor technology,” Oct. 01, 2018, *Elsevier Ltd*. doi: 10.1016/j.nanoen.2018.08.013.

[3] V. S. Marin Halper James C Ellenbogen, “Supercapacitors: A Brief Overview MITRE MITRE MITRE MITRE,” 2006. [Online]. Available: http://www.mitre.org/tech/nanotech

[4] T. Schoetz, L. W. Gordon, S. Ivanov, A. Bund, D. Mandler, and R. J. Messinger, “Disentangling faradaic, pseudocapacitive, and capacitive charge storage: A tutorial for the characterization of batteries, supercapacitors, and hybrid systems,” Apr. 20, 2022, *Elsevier Ltd*. doi: 10.1016/j.electacta.2022.140072.

[5] M. S. Whittingham, R. F. Savinell, and T. Zawodzinski, “Introduction: Batteries and fuel cells,” Oct. 2004. doi: 10.1021/cr020705e.

[6] A. Yu, V. Chabot, and J. Zhang, “Electrochemical supercapacitors for energy storage and delivery: Fundamentals and applications,” *Electrochemical Supercapacitors for Energy Storage and Delivery: Fundamentals and Applications*, pp. 1–355, Jan. 2017, doi: 10.1201/B14671/ELECTROCHEMICAL-SUPERCAPACITORS-ENERGY-STORAGE-DELIVERY-AIPING-YU-JIUJUN-ZHANG-VICTOR-CHABOT/RIGHTS-AND-PERMISSIONS.

[7] A. González, E. Goikolea, J. A. Barrena, and R. Mysyk, “Review on supercapacitors: Technologies and materials,” May 01, 2016, *Elsevier Ltd*. doi: 10.1016/j.rser.2015.12.249.

[8] M. Hashemi, M. S. Rahmanifar, M. F. El-Kady, A. Noori, M. F. Mousavi, and R. B.

Kaner, “The use of an electrocatalytic redox electrolyte for pushing the energy density boundary of a flexible polyaniline electrode to a new limit,” *Nano Energy*, vol. 44, pp. 489–498, Feb. 2018, doi: 10.1016/j.nanoen.2017.11.058.

[9] T. C. Mendes, F. Zhou, A. J. Barlow, M. Forsyth, P. C. Howlett, and D. R. MacFarlane, “An ionic liquid based sodium metal-hybrid supercapacitor-battery,” *Sustain Energy Fuels*, vol. 2, no. 4, pp. 763–771, 2018, doi: 10.1039/c7se00547d.

[10] M. Conte, “Supercapacitors technical requirements fornew applications,” 2010, *John Wiley and Sons Ltd*. doi: 10.1002/fuce.201000087.

[11] R. Dubey and V. Guruviah, “Review of carbon-based electrode materials for supercapacitor energy storage,” *Ionics (Kiel)*, vol. 25, no. 4, pp. 1419–1445, Apr. 2019, doi: 10.1007/S11581-019-02874-0.

[12] S. Najib and E. Erdem, “Current progress achieved in novel materials for supercapacitor electrodes: mini review,” *Nanoscale Adv*, vol. 1, no. 8, pp. 2817–2827, Aug. 2019, doi: 10.1039/C9NA00345B.

[13] J. Xu, S. Zhang, Z. Wei, W. Yan, X. Wei, and K. Huang, “Orientated VSe2 nanoparticles anchored on N-doped hollow carbon sphere for high-stable aqueous energy application,” *J Colloid Interface Sci*, vol. 585, pp. 12–19, Mar. 2021, doi: 10.1016/J.JCIS.2020.11.065.

[14] K. A. S. Raj and C. S. Rout, “Facile synthesis of manganese-doped 2D vanadium diselenide nanosheets for high-performance supercapacitor applications,” *Emergent Mater*, vol. 4, no. 4, pp. 1037–1046, Aug. 2021, doi: 10.1007/S42247-021-00239-W.

[15] X. Zhang, Z. Zhang, X. Zhang, H. Sun, Q. Hu, and H. Wang, “Enhanced supercapacitive energy storage performance of metal organic frameworks derived shuttle-like vanadium selenide in K3Fe(CN)6-based redox electrolyte,” *Journal of Materials Science: Materials in Electronics*, vol. 34, no. 5, Feb. 2023, doi: 10.1007/S10854-022-09682-9.

[16] K. A. Sree Raj, A. S. Shajahan, B. Chakraborty, and C. S. Rout, “Two-Dimensional

Layered Metallic VSe2/SWCNTs/rGO Based Ternary Hybrid Materials for High Performance Energy Storage Applications," *Chemistry - A European Journal*, vol. 26, no. 29, pp. 6662–6669, May 2020, doi: 10.1002/CHEM.202000243;CSUBTYPE:STRING:SPECIAL;PAGE:STRING:ARTICLE/CHAPTER.

[17] K. Chaudhary *et al.*, "Ti3C2Tx MXene reinforcement: a nickel–vanadium selenide/MXene based multi-component composite as a battery-type electrode for supercapacitor applications," *Dalton Transactions*, vol. 53, no. 26, pp. 11147–11164, Jul. 2024, doi: 10.1039/D4DT01230E.

[18] G. Huang, C. Li, X. Sun, and J. Bai, "Fabrication of vanadium oxide, with different valences of vanadium, -embedded carbon fibers and their electrochemical performance for supercapacitor," *New Journal of Chemistry*, vol. 41, no. 17, pp. 8977–8984, Aug. 2017, doi: 10.1039/C7NJ01482A.

[19] G. Wee, H. Z. Soh, Y. L. Cheah, S. G. Mhaisalkar, and M. Srinivasan, "Synthesis and electrochemical properties of electrospun V2O5 nanofibers as supercapacitor electrodes," *J Mater Chem*, vol. 20, no. 32, pp. 6720–6725, Aug. 2010, doi: 10.1039/C0JM00059K.

[20] "Chemistry of Vanadium - Chemistry LibreTexts." Accessed: May 13, 2025. [Online]. Available: https://chem.libretexts.org/Bookshelves/Inorganic_Chemistry/Supplemental_Modules_and_Websites_(Inorganic_Chemistry)/Descriptive_Chemistry/Elements_Organized_by_Block/3_d-Block_Elements/Group_05%3A_Transition_Metals/Chemistry_of_Vanadium

[21] C. Zhong, Y. Deng, W. Hu, J. Qiao, L. Zhang, and J. Zhang, "A review of electrolyte materials and compositions for electrochemical supercapacitors," *Chem Soc Rev*, vol. 44, no. 21, pp. 7484–7539, Nov. 2015, doi: 10.1039/C5CS00303B.

[22] A. Jilani, M. S. Abdel-wahab, A. Hosny Hammad, A. Jilani, M. S. Abdel-wahab, and

A. Hosny Hammad, “Advance Deposition Techniques for Thin Film and Coating,” *Modern Technologies for Creating the Thin-film Systems and Coatings*, Mar. 2017, doi: 10.5772/65702.

[23] O. O. Abegunde *et al.*, “Overview of thin film deposition techniques,” *AIMS Materials Science 2019 2:174*, vol. 6, no. 2, pp. 174–199, 2019, doi: 10.3934/MATERSCI.2019.2.174.

[24] H. M. Pathan and C. D. Lokhande, “Deposition of metal chalcogenide thin films by successive ionic layer adsorption and reaction (SILAR) method,” *Bulletin of Materials Science*, vol. 27, no. 2, pp. 85–111, 2004, doi: 10.1007/BF02708491/METRICS.

[25] M. Sasagawa and Y. Nosaka, “Studies on the effects of Cd ion sources and chelating reagents on atomic layer CdS deposition by successive ionic layer adsorption and reaction (SILAR) method,” *Physical Chemistry Chemical Physics*, vol. 3, no. 16, pp. 3371–3376, Jan. 2001, doi: 10.1039/B101075L.

[26] K. Y. Law, “Definitions for hydrophilicity, hydrophobicity, and superhydrophobicity: Getting the basics right,” *Journal of Physical Chemistry Letters*, vol. 5, no. 4, pp. 686–688, Feb. 2014, doi: 10.1021/JZ402762H/SUPPL_FILE/JZ402762H_LIVESLIDES.MP4.

[27] G. A. Jeffery and B. D. Cullity, *Elements of x-ray diffraction*. Pearson Education Limited, 2014.

[28] M. Birkholz, “Thin Film Analysis by X-Ray Scattering,” *Thin Film Analysis by X-Ray Scattering*, pp. 1–356, May 2006, doi: 10.1002/3527607595.

[29] “X-ray Diffraction (XRD) | Anton Paar Wiki.” Accessed: May 11, 2025. [Online]. Available: https://wiki.anton-paar.com/en/x-ray-diffraction-xrd/

[30] “XRD.” Accessed: May 11, 2025. [Online]. Available: https://rigaku.com/products/x-ray-diffraction-and-scattering/xrd

[31] “Analysis of Thin Films by Infrared Spectroscopy: Review.” Accessed: May 13, 2025. [Online]. Available: https://www.researchgate.net/publication/347623246_Analysis_of_Thin_Films_by_Infrared_Spectroscopy_Review

[32] H. S. Min, “Scanning Electron Microscopy Analysis of Thin Films: A Review,” *Research Aspects in Chemical and Materials Sciences Vol. 5*, pp. 16–28, Dec. 2022, doi: 10.9734/BPI/RACMS/V5/4419E.

[33] G. A. Mabbott, “An introduction to cyclic voltammetry,” *J Chem Educ*, vol. 60, no. 9, pp. 697–702, 1983, doi: 10.1021/ED060P697;JOURNAL:JOURNAL:JCEDA8.

[34] P. T. Kissinger and W. R. Heineman, “Cyclic voltammetry,” *J Chem Educ*, vol. 60, no. 9, pp. 702–706, 1983, doi: 10.1021/ED060P702;ISSUE:ISSUE:10.1021/JCEDA8.1983.60.ISSUE-9;PAGE:STRING:ARTICLE/CHAPTER.

[35] J. W. Gittins *et al.*, “Interlaboratory study assessing the analysis of supercapacitor electrochemistry data,” *J Power Sources*, vol. 585, p. 233637, Nov. 2023, doi: 10.1016/J.JPOWSOUR.2023.233637.

[36] B. Pandit, A. Agarwal, P. Patel, and B. R. Sankapal, “The electrochemical kinetics of cerium selenide nano-pebbles: the design of a device-grade symmetric configured wide-potential flexible solid-state supercapacitor,” *Nanoscale Adv*, vol. 3, no. 4, pp. 1057–1066, Feb. 2021, doi: 10.1039/D0NA00893A.

[37] B. Pandit, A. Agarwal, P. Patel, and B. R. Sankapal, “The electrochemical kinetics of cerium selenide nano-pebbles: the design of a device-grade symmetric configured wide-potential flexible solid-state supercapacitor,” *Nanoscale Adv*, vol. 3, no. 4, pp. 1057–1066, Feb. 2021, doi: 10.1039/D0NA00893A.

[38] M. M. Sajid *et al.*, “Facile synthesis of Se/BiVO4 heterojunction composite and evaluation of synergetic reaction mechanism for efficient photocatalytic staining of organic dye pollutants in wastewater under visible light,” *Journal of Materials*

Science: Materials in Electronics, vol. 31, no. 22, pp. 19599–19612, Nov. 2020, doi: 10.1007/s10854-020-04487-0.

[39] Y. C. Hong and H. S. Uhm, “A Crystalline Material Made from Oxidation of Vanadium Nitride via Foam Route,” *Soft Nanoscience Letters*, vol. 03, no. 04, pp. 83–86, 2013, doi: 10.4236/snl.2013.34015.